Energy & Environmental Science

Accepted Manuscript

ROYAL SOCIETY OF CHEMISTRY

www.rsc.org/ees

Broader Context

Photocatalysis based on semiconductor materials is being actively investigated as a core technology in solar light harvesting and utilizing processes. The basic process is driven by the photoinduced charge transfers (CTs) occurring on the irradiated semiconductor surface with initiating various redox reactions that are utilized for environmental remediation and solar energy storage. The former reaction is usually initiated by a single electron transfer under aerated conditions to generate reactive oxygen species whereas the latter proceeds via two or more electron transfers in the absence of molecular oxygen. Most of the former reaction systems are thermochemically spontaneous ($\Delta G° < 0$) and lead to the mineralization of organic pollutants whereas the latter is an energy uphill process ($\Delta G° > 0$) and often needs co-catalysts to facilitate the multi-electron transfer processes. The mechanisms and kinetics of interfacial/interparticle CTs are influenced by the bulk and surface properties of semiconductor. While various surface modification techniques have been developed so far, their effects are very diverse and even contradictory in some cases. Better understanding of how the modification influences the photoinduced CT events in semiconductors is required, particularly for designing hybrid photocatalysts with controlled CTs, which is sought-after for practical applications of photocatalysis.

Table of Content

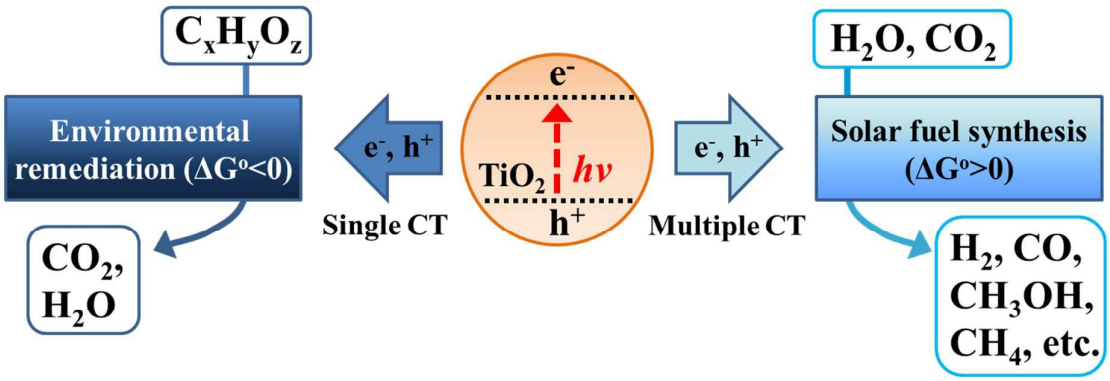

Photoinduced charge transfer processes in solar photocatalysis based on modified TiO_2

Hyunwoong Park,[1] Hyoung-il Kim,[2] Gun-hee Moon,[2] and Wonyong Choi[2]*

[1]*School of Energy Engineering, Kyungpook National University, Daegu 702-701, Korea*

[2]*School of Environmental Science and Engineering, Pohang University of Science and Technology (POSTECH), Pohang 790-784, Korea*

Submitted to

Energy and Environmental Science

(Perspective Article Invited)

Revised

December 2015

* To whom correspondence should be addressed (W. Choi)

E-mail: wchoi@postech.edu

Phone: +82-54-279-2283

Abstract

High efficiency solar photocatalysis requires an effective separation of photogenerated charge carriers and their rapid transport to the semiconductor interface. The mechanisms and kinetics of charge separation and interfacial/interparticle charge transfers (CT) are significantly influenced by both the bulk and surface properties of semiconductor. Surface properties are particularly important because the photocatalysis should be driven by the interfacial CTs. The most popular and the most investigated semiconductor photocatalyst is based on bare and modified TiO_2. This article highlights the interfacial and interparticle CTs under the bandgap excitation of TiO_2 particles, visible light-induced photochemical processes via either dye-sensitization or ligand-to-metal CTs at surface modified TiO_2 particles, and applications of the photo-processes to pollutant degradation and simultaneous hydrogen production. While a variety of surface modification techniques using various nanomaterials and chemical reagents have been developed and tested so far, their effects are very diverse depending on the characteristics of the applied photocatalytic systems and even contradictory in some cases. Better understanding of how the modification influences the photoinduced CT events in semiconductors is required, particularly for designing hybrid photocatalysts with controlled CTs, which is sought-after for practical applications of photocatalysis.

1. Introduction

Solar energy is the main driver of most biological and global environmental processes. In addition, the need of harvesting and utilizing sunlight as a renewable source of energy is continuously increasing. Solar photocatalysis based on semiconductor materials has been extensively studied over the past four decades and is still being actively investigated as a core technology in solar light harvesting and solar conversion processes.[1-11] The basic process is driven by the photoinduced charge transfers occurring on the irradiated semiconductor surface with initiating a variety of redox conversion reactions. Most of semiconductor photocatalytic processes have been studied for the production of solar fuels (*e.g.,* H_2) and the environmental purification of contaminated water and air.[2-9] As the cost of fossil fuels and the demand for advanced environmental remediation technologies increase, the fundamental studies on photocatalysis[12-16] as well as its practical applications[6,17] have received growing attention.[18] A bibliographic database web-engine (Scopus) search finds over 7,500 and 3,500 publications in 2014 alone for the search keywords of photocatal* and TiO_2* photocatal*, respectively, which reflects the continued popularity of this research field.

A variety of semiconductor photocatalysts (TiO_2,[4,5,7,8,10,19] ZnO,[20-22] WO_3,[23-27] Fe_2O_3,[28] $BiVO_4$,[29-31] CdS,[25,32-34] CdSe,[35] etc.) with different morphologies and modifications have been studied and developed. The photocatalysis is initiated by the light absorption of semiconductor, followed by the charge-pair separation and interfacial charge transfer (CT). Since these reactions primarily occur on the surface, the modifications of semiconductor surface structures and properties significantly influence the overall photocatalytic reaction kinetics and mechanisms.[7,8] Imbalance of

the interfacial CTs of electrons and holes causes the charge pairs to rapidly recombine with each other, reducing or even nullifying the overall photocatalytic activity of interest. In this regard, proper understanding of the behavior of photogenerated CTs is necessary to achieve the desired reactions with high efficiency. With advancements in the fundamental studies on charge carrier dynamics,[16] the behaviors of photogenerated charge carriers have been more clearly elucidated. This helps us understand how surface modification affects the photocatalytic processes in different ways, and eventually control the photocatalytic pathways and activity.

The CT reactions occurring on semiconductor photocatalysts have been applied for two main purposes: (1) environmental applications for the remediation of polluted water and air and (2) solar energy storage through the synthesis of solar fuels (*e.g.,* H_2 production from water splitting, CO_2 conversion to hydrocarbons). Scheme 1 illustrates how the characteristics of CTs in the two processes are different. The former process is usually initiated by a single electron transfer under aerated conditions to generate reactive radical species whereas the latter proceeds via two or more electron transfers in the absence of molecular oxygen (O_2). Generally, the photocatalytic degradation of organic compounds does not proceed in the absence of O_2, whereas the photocatalytic production of solar fuels (*e.g.,* H_2, HCOOH) is very difficult to be achieved in the presence of O_2 because the molecular oxygen scavenges photogenerated electrons.[36] Most of the former reaction systems are thermochemically spontaneous ($\Delta G° < 0$) and lead to the mineralization of organic pollutants whereas the latter for solar fuel synthesis is an energy uphill (energy-storing) process ($\Delta G° > 0$) and often needs co-catalysts (e.g., Pt,[37] Pd,[38] Co,[29,39,40] Ni,[41,42] Sn,[43] Mn[44]) to facilitate the multi-electron transfer processes.

Some outstanding questions related with CTs on semiconductor photocatalysts are as follows: 1) How can the recombination of charge pairs be minimized? 2) How can the single-electron transfer and the multi-electron transfer processes be controlled? 3) What determines the pathways of hole (or electron) transfer reactions leading to the generation of reactive radical species such as hydroxyl radical, superoxide, or singlet oxygen? Is it possible to control this selectively and if so, how? 4) How can visible light photons be utilized to induce CT in semiconductor photocatalysis? Such questions and the related research topics are listed as an example in Table 1. With these in mind, this article discusses the photoinduced CTs occurring on semiconductor photocatalysts modified with various methods developed by this research group and addresses the above questions.

2. Interfacial charge transfers

The interfacial CT characteristics required as a photocatalyst for environmental remediation and those as a photocatalyst for solar-fuel synthesis should be different. The former is mainly based on a single-electron transfer process, which accompanies the generation of reactive oxygen species (ROS) such as hydroxyl radical and superoxide (Fig. 1). On the other hand, the latter (solar fuel synthesis) proceeds through a multi-electron transfer process to synthesize energy-rich molecules (*e.g.,* H_2, CH_3OH, CO, NH_3) through the activation of thermochemically very stable precursors (*e.g.,* H_2O, CO_2, N_2). Under the condition of limited solar flux, the transfer of multiple electrons and holes should be done through a sequential process of single electron transfers,

which must involve various intermediate species. Since the intermediates are usually unstable and short-lived, the efficiency of multi-electron transfer is much lower than that of the single-electron transfer process.[45] Since the CT characteristics are very different depending on the application purposes, a photocatalyst that is good for the degradation of organic pollutants can be poor for the solar fuel production if the single electron transfer is predominantly favored with a specific photocatalyst. The same can be said for the reverse case. The photochemical generation of ROS and the multi-electron transfer processes for fuel synthesis are vitally important in determining the photocatalytic activity but the detailed understanding of this critical process at the molecular level is still far from complete and the methods to control the CT behavior are limited.

Incidentally, considering that the earth crust is mainly composed of metal oxides including potentially photoactive ingredients like iron oxides, it is interesting to note that their lack of significant photoactivity under solar irradiation seems to be desirable to make the earth environment habitable for life. Efficient generation of ROS on solar irradiated metal oxides (soils and rocks) would have destroyed organic matters and microorganisms. If water splitting had occurred on sunlit metal oxides, it might have changed the atmospheric composition that would be different from the current one (*e.g.,* elevated H_2 concentration in the atmosphere).

2.1. Charge transfers and the accompanying production of reactive species

2.1.1. **Valence band (VB) holes**. The irradiation of semiconductors excites an electron from VB to conduction band (CB) with leaving a hole (h^+) in the VB and the oxidizing power of the hole often destabilizes the semiconductor material itself, which limits the

practical application of semiconductor photocatalysts. In this respect, TiO_2 is an excellent material that exhibits good photocatalytic activity and long-term stability in a wide pH range under both dark and irradiation conditions.[8] A fraction of photogenerated holes surviving the rapid recombination process diffuse to the semiconductor surface where they can react with any electron-donating species, which is a main driving force of most photocatalytic oxidation (PCO) processes. The reaction of the holes depends on both their oxidizing potential and the availability of adsorbed substrates. The holes readily react with strongly adsorbing molecules such as formate and oxalate (*i.e.,* electron donors) whereas they are less reactive with weakly adsorbing molecules (*e.g.,* chlorinated ethanes, chlorophenols).[46-51] The hole oxidation potential is essentially equal to the VB edge potential and depends on the kind of semiconductors. Semiconductors with wide bandgap usually have highly positive VB potentials and the VB edge of TiO_2 that lies around ~2.7 V (*vs.* NHE at pH 7) induces the generation of strongly oxidizing holes under UV irradiation. The VB positions of metal oxide semiconductors like TiO_2 are usually similar among themselves because the VB consists mainly of O 2p orbital that is a common component of oxide materials.[12,52] However, TiO_2 is unique not only in its highly oxidizing VB hole but also its excellent (photo)chemical stability, abundance and low material cost, and non-toxicity, which distinguish itself from other oxide semiconductors.

The oxidation power of photogenerated holes can be modified when impurity dopants (*e.g.,* transition metal ions, N, C) are introduced into the TiO_2 lattice to create extra energy levels within the forbidden bandgap. Owing to the less positive levels of the dopants energy states in comparison to the original VB edge, the oxidizing power of

holes trapped at the dopant sites is less energetic.[53,54] This is why the visible light photocatalytic activities of doped TiO_2 are often limited compared with that of UV/TiO_2.[55-58] For example, nitrogen-doped TiO_2 failed to catalyze the oxidation of formate ($HCOO^-$) (reaction 1) under visible irradiation ($\lambda > 400$ nm) although it can absorb visible light up to ~600 nm.[55]

$$HCOO^- + h^+/{}^\bullet OH \rightarrow H^+/H_2O + CO_2^{\bullet -} \quad (1)$$

This was confirmed by the absence of $CO_2^{\bullet -}$ adduct with DMPO (5,5-dimethyl-1-pyrroline N-oxide) in the electron spin resonance spectra under visible light irradiation. Similarly to this, the major oxidant in the photocatalysis of carbon-doped TiO_2 was suggested to be holes in the midgap states,[57] the potential of which is strong enough to directly oxidize 4-chlorophenol ($E^0 = 0.8$ V) but not enough to generate $^\bullet$OH ($E^0 = 2.7$ V). Metal-doped TiO_2 samples exhibited the same phenomena. The photocatalytic degradation of tetramethylammonium (TMA: a probe substrate that can be degraded by $^\bullet$OH radical) can be successfully achieved with bare TiO_2 under UV irradiation, whereas the visible activity of Pt_{ion}-TiO_2 (Pt-doped) for the TMA degradation was negligible.[56] It is often regarded that the development of efficient visible light active photocatalysts is an ultimate goal in photocatalysis research but it should be realized that the available photocatalytic redox power under visible irradiation is sacrificed at the expense of utilizing lower energy photons, which limits the range of redox reactions that can be driven photocatalytically. The visible light photocatalysts are highly desired for solar conversion purposes but they are not a panacea.

2.1.2. **Hydroxyl radicals**. The most common hole trapping site on the metal oxide surface is the surface hydroxyl group and the hydroxyl radical is generated as a result of a hole reaction with a surface hydroxyl group or an adsorbed water molecule. The hydroxyl radical is one of the most powerful oxidants and reacts non-selectively with most organic substrates either via the abstraction of H atom ($H^{\bullet}$) from C-H bonds or via the addition to double bonds and aromatic rings. The resulting carbon-centered radical species (generated from the reaction with $^{\bullet}OH$) subsequently combines with O_2 at a diffusion-limited rate to produce alkyl peroxy radicals which are eventually transformed into CO_2. The $^{\bullet}OH$-mediated PCO of refractory organic pollutants including polychlorinated dibenzo-p-dioxins (PCDDs),[59,60] TMA,[23,56,61-63] carbon soot[51,64] are good examples demonstrating the superior oxidative power of OH radicals generated in PCO process.[50,59]

The role of OH radicals in PCO processes is widely accepted and the photocatalytic degradation of pollutants on UV-illuminated TiO_2 through their action has been demonstrated for a great number of organic compounds. The OH radicals generated on illuminated TiO_2 are present mainly in the form of surface bound hydroxyl radical ($\bullet OH_s$).[4,8] However, it has been demonstrated that some fraction of OH radicals desorb from the surface as an unbound radical (free, $\bullet OH_f$) and diffuse into the reaction medium. The previous studies investigated the desorption of $\bullet OH_f$ at the TiO_2/air interface[51,65-72] and clearly demonstrated that the OH radicals generated from illuminated TiO_2 diffuse through the air to react with a substance that is not in direct contact with TiO_2 surface. The diffusing radicals react with various remote substrates (*e.g.,* carbon soot,[51,64,67,73] stearic acid,[64] polymer[71]) and were demonstrated even to pass

through an organic polymer membrane of ~120 μm thickness.[68] The desorption of OH radicals is also allowed at the TiO_2/*water* interface, which was confirmed by a recent study that observed the diffusing $•OH_f$ from the illuminated TiO_2 surface *in water* through a gap of 7.5 μm using a single molecule detection technique based on total internal reflection fluorescence microscopy (TIRFM).[74] In PCO processes, the hole and $•OH_s$ react mainly with adsorbed substrates and the desorption of intermediates from the surface should inhibit further mineralization. On the other hand, mobile $•OH_f$ can react with both surface-bound and unbound substrates/intermediates and is a more versatile oxidant. The $•OH_f$ diffusing from the irradiated anatase TiO_2 into the aqueous bulk was observed while that was not observed with rutile as shown in Fig. 2a and 2b. Therefore, the PCO on rutile is largely limited to the adsorbed substrates whereas the working range of PCO on anatase is more expanded owing to the presence of mobile •OH (Fig. 2c). This mechanism was newly suggested as an explanation for the common observations that anatase has higher activities than rutile for many PCO reactions. Therefore, as for the photocatalytic reductive conversion that does not involve the hydroxyl radical, the intrinsic activities of anatase and rutile are little different.[73] However, why anatase allows the desorption of $•OH_f$ and rutile does not and what properties of the TiO_2 surface control the desorption of the active radical at the molecular level are not understood and need to be further explored.

The generation of OH radicals can be changed by modifying the surface of semiconductor. The surface adsorption of inorganic anions (fluorides, phosphates, and sulfates) may be the simplest method.[75,76] The surface fluorination of TiO_2, which replaces the surface hydroxyl group with fluoride (reaction 2),[77-82] was suggested to prefer the generation of $•OH_f$ to $•OH_s$ because VB holes react mainly with the adsorbed

water molecules (not the surface hydroxyl group) under the condition that the surface hydroxyl groups are depleted by the fluoride substitution.[83]

$$>\text{Ti-OH} + \text{F}^- \rightarrow >\text{Ti-F} + \text{OH}^- \quad (p\text{K}_\text{F} = 6.2) \qquad (2)$$

The surface fluorination also hinders the direct VB hole transfer pathway when the presence of surface fluoride inhibits the adsorption of substrates.[75,77-80] Free OH radicals that desorb from the TiO_2 surface have high mobility and diffusivity in the aqueous solution.[8,51,72] Hence the photocatalytic decompositions of phenol,[75] TMA,[62] and acid orange 7[75] were enhanced on the fluorinated TiO_2. On the other hands, the hole transfer-mediated oxidations are significantly retarded because the adsorption or surface complexation of substrates is usually inhibited on the fluorinated surface.[75] Such enhanced OH radical-mediated pathway on the fluorinated surface was further confirmed by the highly accelerated photocatalytic degradation of stearic acid film that is remotely located ~150 μm away from the fluorinated TiO_2 surface through the air.[65] The adsorption of phosphates and sulfates on TiO_2 may exhibit similar effects[76,79,80] despite the difference in the working pH region, effectiveness, and stability.

2.1.3. **Conduction band (CB) electrons**. Although the VB holes and OH radicals are the main active species in most PCO processes, their roles are effective only when the CB electrons are also efficiently transferred on the illuminated semiconductor surface. Otherwise, the accumulation of CB electron results in the fast recombination with VB holes or surface-bound OH radicals, which reduces the overall photocatalytic efficiencies. As for TiO_2, the CB edge is located at ca. –0.51 V (at pH 7), which gives CB electrons a mild reducing power. In most PCO processes, molecular oxygen

dissolved in water or in ambient air serves as a scavenger of CB electrons ($E°(O_2/O_2^{\bullet-}$ = –0.33 V). The presence of alternative electron acceptors such as Fe^{3+},[37,84,85] Ag^{+},[86,87] H_2O_2,[88,89] $S_2O_8^{2-}$,[88,90-92] BrO_3^-,[88,90] IO_4^-,[88,90,91] and polyoxometalate (POM)[37,85,93-96] may accelerate the photocatalytic processes and enable some photocatalytic processes even in the absence of O_2. While the transfer of CB electrons to O_2 induces the generation of ROS such as superoxide and hydrogen peroxide, the direct CB electron transfer to some substrates may induce their reductive transformation or degradation. For example, perhalogenated compounds such as carbon tetrachloride (CCl_4),[97,98] trichloroacetate ($CCl_3CO_2^-$; TCA),[99] and perfluorooctanesulfonic acid (PFOS)[100-103] hardly react with the VB holes and OH radicals because of the lack of the oxidizable functional groups such as C-H bonds and unsaturated bonds. Such compounds should be reductively degraded through CB electron transfers (e.g., *see* reaction 3). The CB electron transfer part is also critical in the transformation of inorganic substances such as inorganic oxyanions and metal ions. A typical example is the reductive transformation of toxic metal ions to lower oxidation states (e.g., Cr(VI) →Cr(III))[104,105] or to the zero-valent metallic state (e.g., Ag(I) → Ag^0)[104,105] through successive single electron transfers.[106,107]

The electron transfer part can be also controlled by modifying the TiO_2 surface. Surface platinization is the most commonly employed technique for enhancing the CB electron transfer.[108] When Pt is deposited onto TiO_2 with creating a Schottky barrier at the interface,[109] the Pt phase on TiO_2 serves as an electron sink, facilitating the charge separation and retarding charge recombination. The enhanced electron transfer on Pt-deposited TiO_2 has been demonstrated in many cases. The electron shuttles (e.g.,

Fe^{3+}/Fe^{2+} redox couple) present in the illuminated suspension of semiconductor particles can generate current on a collector electrode and the deposition of Pt on suspended TiO_2 particles markedly enhanced the photocurrent (Fig. 3), which demonstrates the role of Pt in facilitating the interfacial electron transfer.[37] The accelerated dechlorination of CCl_4 in dye-sensitized Pt/TiO_2 suspensions is also a good evidence of the role Pt as an electron transfer mediator.[97,98]

$$CCl_4 + e^-_{cb}\,(Pt/TiO_2) \rightarrow \bullet CCl_3 + Cl^- \qquad (3)$$

The scavenging of electrons in Pt subsequently accelerates the hole-mediated oxidation part as demonstrated in numerous cases.[8,79,99,110-115] The overall transfer of electrons and holes on semiconductor nanoparticles should be balanced to maintain the charge neutrality. However, the role of Pt is more complex than that of a simple CB electron sink. The presence of Pt not only accelerates the photocatalytic reaction rate but also changes the reaction pathways to generate different products because of the well-known thermal catalytic activity of Pt.[99,114,116] In addition, the Pt effects on the photocatalysis rate are not always positive and negative effects were also reported.[99,115] To make the matter more complex, the reported Pt effects on the photocatalytic degradation of a specific substrate are often contradictory.[117-121] In other words, the Pt effects are highly substrate-specific and depend on the Pt-substrate interaction as well as the intrinsic properties of Pt (size, oxidation state, etc). For example, the oxidation state of Pt critically influences the initial degradation rate of trichloroethylene (TCE).[115] While the photocatalytic activity of Pt^0/TiO_2 is almost similar to that of bare TiO_2, TiO_2 loaded with oxidized Pt (Pt_{ox}) exhibits negligibly low activity. It was proposed that TCE adsorbed on Pt_{ox} chemically mediates the charge recombination through the redox cycle

of TCE. The platinization of TiO_2 and other semiconductors as a mean of enhancing the photocatalytic activity has been very popular but the overall effects are rather complex and not easy to be generalized. It depends on how the platinized samples are prepared, what the experimental conditions are, and what the substrates are. The effects of the presence of Pt on the semiconductor photocatalytic reactions, though widely practiced and popular, still need to be understood at the molecular level.

2.1.4. **Superoxide and hydroperoxyl radicals**. The formation of superoxide (O_2^-) through a CB electron transfer to O_2 is thermodynamically favorable since the TiO_2 CB edge potential (–0.51 V at pH 7) is slightly more negative compared to the reduction potential of O_2 (–0.33 V). With increasing pH, the position of the CB edge moves by -59 mV per unit pH (*Nernstian* behavior) owing to the amphoteric nature of the surface hydroxyl groups on TiO_2, whereas the reduction potential of O_2 is unchanged. As a result, the thermodynamic driving force for electron transfer becomes greater with increasing pH. With decreasing pH, hydroperoxyl radicals (HO_2) become the predominant species, owing to the acid-base equilibrium between HO_2 and O_2^- ($HO_2 \leftrightarrow O_2^- + H^+$; $pK_a = 4.8$).[122] From the kinetics point of view, the CB electron transfer to O_2 is much slower (~milliseconds) than that of hole transfer (~100 nanoseconds) at the TiO_2 interface, suggesting that the CB electron transfer part can limit the overall PCO reaction rate.[4,123,124]

The superoxide/hydroperoxyl radical is generally a much weaker oxidant than VB hole and OH radical but it can serve as an important oxidant in some cases. An outstanding example is the PCO of arsenite (As^{III}) to arsenate (As^{V}).[96,125-129] It has been proposed[96,126,127,129,130] and later verified[125,128] by time-resolved transient absorption

spectroscopy that the arsenite adsorbed on TiO_2 serves as an external charge-recombination center, where the reaction of arsenite with holes and OH radicals is immediately followed by a CB electron transfer (Fig. 4). Although the trapped electron transfer to O_2 is slow (> 20 μs) and the homogeneous bimolecular rate constant between superoxide and arsenite is as low as 10^6 $M^{-1}s^{-1}$, the presence of As^{IV}/As^{III} redox couple-mediated null cycle makes the superoxide-mediated oxidation path important in the photocatalytic conversion of As^{III} to As^{V}. The modification of TiO_2 surface may enhance the electron transfer to O_2 and inhibits the As^{IV}/As^{III} couple-mediated null cycle with significantly changing the PCO kinetics of arsenite. For example, the loading of co-catalysts such as Pt on TiO_2 facilitates the electron transfer to O_2 with enhancing the generation of superoxide and accelerating the PCO of arsenite. TiO_2 hybridized with reduced graphene oxide (rGO) works similarly as Pt/TiO_2 and facilitates the transfer of photo-generated electrons from TiO_2 CB to O_2, which subsequently hinders the As^{IV}/As^{III}-mediated recombination and enhances the overall arsenic oxidation.

2.1.5. **Hydrogen peroxide**. The solar photocatalytic production of hydrogen peroxide (H_2O_2) is interesting in view of both environmental and energy applications. It is not only a widely used oxidant in water treatment processes but also a valuable fuel itself with a high energy content. Hydrogen peroxide is generated by the proton-coupled electron transfer to superoxide and hydroperoxyl radical ($E^o(HO_2^\bullet/H_2O_2)$ = 1.007 V at pH 7). It can also be produced from the recombination of two OH radicals but this process is a minor pathway in aqueous photocatalytic systems.[131] In contrast with ZnO, the amount of H_2O_2 produced on TiO_2 is very small (< 0.1 μM) even in the presence of organic electron donors, because it forms the surface peroxo species on TiO_2 which is

immediately degraded under irradiation.[17,132] The photocatalytic production of H_2O_2 can be significantly enhanced by either facilitating the interfacial electron transfer or suppressing the adsorption of in-situ generated H_2O_2. For example, Au nanoparticles loaded on TiO_2 facilitate the reduction of molecular oxygen,[133] while the surface fluorides on TiO_2 effectively inhibit the formation of surface peroxide species,[82] both of which significantly enhances the overall production of H_2O_2 under UV irradiation. The in-situ produced H_2O_2 can be decomposed into hydroxyl radicals and hydroperoxyl radicals via further electron transfer, direct photolysis, or a Fenton-like reaction. It should be noted that H_2O_2 itself serves as both an electron acceptor and an electron donor on illuminated TiO_2. Therefore, the photocatalytic decomposition of H_2O_2 is not retarded at all in the absence of O_2.[134] As a result of H_2O_2 decomposition at the irradiated TiO_2/air interface, HO_2 radicals are produced as an intermediate, some of which desorb from the TiO_2 surface into the gas phase.

2.2. Multiple charge-transfers

2.2.1. Proton-coupled electron transfers (PCETs). The photocatalytic production of H_2 and hydrocarbons through water splitting and CO_2 reduction requires a series of proton-coupled electron transfers (Fig. 5). For example, two electron transfers are necessary for the production of H_2 from water, whereas two, four, six, and eight electron transfers are required for the production of formate, formaldehyde, methanol, and methane from CO_2, respectively. From a thermodynamic point of view, multi-electron transfer is more favorable than single electron transfer (*e.g.,* $E^{\circ}(CO_2/HCOOH) = 0.197$ V) *vs.* $E^{\circ}(CO_2/CO_2^{\bullet -}) = -1.9$ V).[135-139] However, the former is kinetically and stochastically hindered primarily because the supply of electrons is limited by the flux

of incident photons under solar irradiation condition (*not allowing simultaneous multi-photons absorption by a single semiconductor particle*) and the lifetime of the charge transfer intermediates is usually not long enough to wait for the next available electron. As a result, the PCETs should proceed through a series of single electron transfer events, which indicates that the overall photoconversion should involve several intermediates through the sequential electron transfers. The intermediates are usually unstable and short-lived and are subject to the attack from VB holes and OH radicals before reacting with the next electron, which nullifies the overall photoconversion process. On the other hand, unlike the case of water reduction in which H_2 is the sole product, the selectivity control among various CO_2 reduction products remains as a big challenge. The electrochemical reduction potentials of CO_2 through two to eight electron transfers (resulting in diverse products, *see* Fig. 5) fall in a narrow potential range of ~0.4 V and the preferential control for a specific product is difficult thermodynamically. Therefore, the development of catalytic materials for the product selectivity in PCET processes is highly desired.

2.2.2. Catalysts for PCETs. The surface properties of semiconductors have been modified to facilitate and control the multi-electron transfers. TiO_2 is activated only by UV irradiation and its theoretical solar conversion efficiency for hydrogen production (i.e., solar-to-hydrogen (STH) efficiency) is only ~1%.[140] The CB electron in TiO_2 has only mild reduction power, which is not very suitable for the synthesis of solar fuels. However, TiO_2 is still frequently employed as a base material in the solar fuel production owing to its excellent stability, low cost, and low toxicity of the material. To accelerate the multiple CTs, noble metal nanoparticles (Pt, Au, Ag, Ru, and Rh) are

often deposited on semiconductor surfaces, which serves as a reservoir of electrons. Among them, Pt shows the best performance for H_2 evolution due to its ability to attract and store electrons and its optimal catalytic activity for H_2 formation and desorption.[45,141,142]

The presence of Pt is often essential for multi-CTs but its high cost hinders its widespread practical applications. Alternative co-catalytic materials consisting of earth-abundant elements are being actively sought and carbon-based materials including carbon nanotubes,[33,35,143,144] graphite,[145] and graphene[146] have been frequently investigated for this purpose. Such carbon-based materials have unique electronic properties, owing to the conjugated sp^2 carbon networks facilitating CT.[147] For example, reduced graphene oxide (rGO) was shown to serve as an electron reservoir in TiO_2 photocatalysis, retarding the recombination of charge pairs and leading to enhanced photoconversion efficiency (Fig. 6).[145,148,149] In a typical preparation of TiO_2/rGO hybrid, TiO_2 particles were loaded on the rGO sheet but different geometrical arrangements between rGO and TiO_2 particles have a strong influence on the photocatalytic activity.[147,150,151] The hybridization of nanometer-sized GOs and TiO_2 nanoparticles induces a self-assembled core/shell structure which highly enhances the interfacial contact between them in comparison with the particles-on-a-sheet geometry. GO in direct contact to TiO_2 can be photocatalytically reduced, which leads to the formation of TiO_2/rGO core/shell (Fig. 6a). This composite clearly differentiates itself from the conventional TiO_2/rGO composite that is based on the larger μm-sized rGO sheet (particles-on-a-sheet: TiO_2/rGO sheets). The photocatalytic activities of the core/shell are significantly higher than that of bare TiO_2 for hydrogen production (Fig.

6b). In another geometry, TiO_2 nanofibers (NFs) in which GO sheets were incorporated within the NF matrix (GO-TiO_2 NFs) were also prepared and tested for their photocatalytic and PEC activities (Fig. 6a). The GO sheets embedded in TiO_2 NFs improve the interparticle connection and facilitate the charge pair separation by serving as an *in-built* electron conduit with enhancing the photoactivity (Fig. 6c).[152] Even though the photocatalytic activities of TiO_2 hybridized with various forms of carbon nanomaterials are higher than that of bare TiO_2 in many reported cases including the above examples, they are usually lower than that of Pt/TiO_2. However, the co-presence of carbon nanomaterials along with Pt further enhances the photocatalytic activities of Pt/TiO_2. The simultaneous loading of Pt and rGO on TiO_2 (ternary hybrid) markedly enhanced photocatalytic production of H_2, as compared to the binary hybrids (Pt/TiO_2 and TiO_2/rGO) (Fig. 6b). This indicates that rGO can act as an auxiliary co-catalyst, thereby reducing the amount of expensive Pt required for H_2 production.

In addition, rGO was found to be an excellent catalyst to drive photocatalytic production of H_2O_2 in aqueous TiO_2 suspension.[151] rGO/TiO_2 displayed the highest photocatalytic activity in producing H_2O_2 (via PCETs to molecular oxygen) in aqueous 2-propanol solution compared with noble metal-loaded TiO_2 (Fig. 7a). The leveling-off of H_2O_2 production is attributed to the *in-situ* decomposition of produced H_2O_2 and the relevant kinetics can be expressed with $[H_2O_2] = (k_f/k_d)[1 - \exp(-k_d \cdot t)]$ (k_f and k_d referring to the formation and decomposition rate constants, respectively).[131,153] According to the kinetic analysis, k_f with rGO/TiO_2 was not the largest whereas k_d with rGO/TiO_2 was the smallest, leading to the highest net yield of H_2O_2 production. The photocatalytic decomposition of H_2O_2 can be further retarded by adsorbing phosphate

on rGO/TiO_2 because the adsorbed phosphate inhibits the adsorption of H_2O_2 (Fig. 7b). When Co^{2+} was present together with phosphate, cobalt-phosphate complexes (CoPi) were in-situ formed on rGO/TiO_2 (Fig. 7c). The ternary rGO/TiO_2/CoPi produced H_2O_2 at ~80 μM in the absence of any sacrificial hole scavenger, which was far more efficient than rGO/TiO_2 (Fig. 7b).

Other materials can be employed as a modifier of TiO_2 for enhancing the multiple CTs. For the conversion of CO_2 to hydrocarbons, for example, a thin nafion layer can be coated on the Pd/TiO_2 nanoparticles to facilitate PCETs as well as to inhibit the re-oxidation of the intermediates and products.[154] It was found that the introduction of the nafion layer enhanced the production of methane, ethane, and propane in UV-irradiated Pd/TiO_2 suspensions. The effect of the nafion overlayer on TiO_2 seems to be related with its roles to maintain the local proton activity within the layer to facilitate PCET reactions (as a proton conductor) and to inhibit the photooxidation of the intermediate products of CO_2 reduction (as a barrier layer for the oxidation of reaction intermediates). The nafion layer may stabilize the intermediates, inhibit the re-oxidation of the CO_2 reduction products, and subsequently assist in the serial electron transfers to produce the final products. The perfluorinated backbone of nafion itself resists the photooxidation and therefore, the photoactivity of the nafion/Pd/TiO_2 composite can be sustained under UV irradiation. Incidentally, owing to the cation exchange property of nafion, the nafion-coated TiO_2 has been also employed as a photocatalyst that selectively adsorbs cationic substrates or cationic sensitizers.[94,95]

To achieve the overall photoconversion, the PCET half reactions should be coupled with the oxidation half reactions which supply the protons and electrons. The

most ideal counterpart should be the oxidation of water, which also involves the multi-electron transfers (requiring four proton/electron couples) and should be also limited by the photon flux. The photooxidation of water is an important building block in photosynthesis because it is the only reaction that can supply the electrons and protons for a global-scale production of solar fuels.[17,155-157] Although the VB holes in most oxide semiconductors have the oxidation potential high enough to drive the water oxidation, the water oxidation part always kinetically limits the overall photoconversion. In most photocatalytic oxidation processes occurring on bare metal oxide semiconductors, the oxidation of water preferentially generates the transient hydroxyl radical species which has little chance to be further oxidized to O_2 via multiple hole transfers. To overcome this problem, water oxidation catalysts such as cobalt phosphate (CoPi) and nickel borate (NiBi) complexes can be deposited on the semiconductor electrode (mostly non-TiO_2 electrodes such as $BiVO_4$).[29,30,158] The application of anodic biases to the semiconductor electrode oxidizes the deposited cobalt(II) and nickel(II) species (*e.g.*, $Co^{2+} + 2h^+ \rightarrow Co^{4+}$), which form complexes with phosphate and borate under illumination. The oxidized species then return to their original oxidation state through oxidizing water (*e.g.*, $Co^{4+} + H_2O \rightarrow Co^{2+} + 1/2O_2 + 2H^+$). Although this catalytic material is composed of earth-abundant elements and easy to be prepared, it can serve as a charge recombination center because of the sluggish interfacial hole transfer under certain conditions (e.g., large anodic bias, thick coat, etc).[29,41] Incidentally, the water photooxidation on semiconductor electrode can be also enhanced by passivation the semiconductor surface by a thin insulating overlayer, which reduces the number of electron trapping sites on the semiconductor surface, thereby facilitating

water photooxidation despite the insulating nature of the overlayer (e.g., a thin Al_2O_3 overlayer on WO_3 photoanode surface).[159]

3. Interparticle charge transfers

Efficient charge separation can be achieved by interparticle CTs through particle-to-particle junctions. The interparticle CT reduces the chance of charge recombination and eventually increases the overall photocatalytic activities. It occurs both in single semiconductor systems (e.g., agglomerates of colloidal nanoparticles,[160,161] compactly packed nanoparticles[162,163]) and in hybrid semiconductor-composite systems (binary[26,32,164,165] and ternary hybrids[25]). Colloidal or suspended semiconductor particles exist almost always as agglomerates in aqueous solution. Hence, the effects of the agglomerate state on the charge separation and transfer need to be carefully considered. The agglomeration of semiconductor particles is usually thought to have a negative effect on the photocatalytic activity because of the reduced surface area and the enhanced light scattering loss. However, the overall effect of agglomeration seems to be more complex than thought.

3.1. Homojunction semiconductor systems

A recent study reported that the photocatalytic H_2 production in TiO_2 suspension containing nitric acid is greatly accelerated after some induction period (Fig. 8a).[160] This unique phenomenon was attributed to the pH increase resulting from the in-situ photocatalytic reduction of nitrate to ammonia. As the solution pH approaches the zero point charge of TiO_2 (pH_{zpc} ~ 6.9), a rapid agglomeration of TiO_2 colloid is induced,

which initiates the production of H_2. The colloid agglomeration and the appearance of H_2 production is coincident. A similar behavior was observed in the case of photocurrent generation (mediated by the MV^{2+}/MV^{+} redox couple; $E° = –0.445$ V) in TiO_2 colloids: a rapid increase in the photocurrent was observed after the agglomeration of TiO_2 nanoparticles. A plausible explanation is that the charge separation is facilitated by electron hopping from particle to particle when TiO_2 nanoparticles are connected with each other within the agglomerates. Hence, the agglomeration-induced acceleration of H_2 and photocurrent generation is ascribed to the facilitated charge separation by interparticle CT within the agglomerates.

The effect of interparticle CTs in the agglomerates of dye-sensitized TiO_2 nanoparticles was also systematically studied by using both static photocatalysis and transient laser spectroscopy.[161] A typical dye-sensitized system for H_2 production includes dye-sensitized TiO_2 nanoparticles (Dye/TiO_2) as a light absorber and platinized TiO_2 (Pt/TiO_2) as an active catalytic center. Fig. 8b compares two experimental cases of dye sensitization: a common case where the light absorbing dye and the Pt catalyst are on the same nanoparticle (Dye/TiO_2/Pt) and the other case where each part is separated in different nanoparticles and bare TiO_2 nanoparticles are added to mediate between two active parts (Dye/TiO_2 + TiO_2 + Pt/TiO_2). When the light absorbing part of Dye/TiO_2 is separated from the active catalytic center of Pt/TiO_2, the role of bare TiO_2 nanoparticles working as a mediator that connects the above two parts in the agglomerates should be essential. The presence of mediator in the agglomerate indeed facilitated the charge separation (i.e., retarding charge recombination between the oxidized dye and the injected electrons) and the electron transfer from Dye/TiO_2 to Pt/TiO_2 through multiple

grain boundaries subsequently produced more H_2 (Fig. 8b). A similar phenomenon was also observed in the case of dye-sensitized reduction of Cr(VI) to Cr(III):[161] a notable enhancement of Cr(VI) reduction was observed when bare TiO_2 nanoparticles were incorporated as a mediator in the dye-sensitized TiO_2 system. Transient absorption spectroscopic measurements revealed the role of the mediator TiO_2 nanoparticles by monitoring the transient absorption decay of the photogenerated dye cation ($Dye^{\bullet+}$). An increase in the bare TiO_2 amount (as a mediator in the dye-sensitized TiO_2 system) enhanced the average lifetimes (τ) of the dye cation by ~18 times (from 6.7 μs to 120 μs) in the aggregated state (Fig. 8b inset).

To utilize the interparticle CT phenomenon in practical applications, particulate mesoporous TiO_2 (meso-TiO_2) with well-ordered pore structures and unique morphologies was developed without the use of templates via the hydrothermal method (Fig. 9a).[162] The formation of meso-TiO_2 is governed by the electrostatic potential, which can be controlled by the ionic strength of the solution. By changing the solution ionic strength (*e.g.*, by adding KCl), which controls the hydrolysis of the titanium alkoxide precursor, a mesoporous structure consisting of densely packed nanoparticles was synthesized. The as-synthesized meso-TiO_2 microspheres (0.5 – 1 μm) consisting of small primary nanoparticles (10 – 15 nm) exhibit markedly enhanced photo(electro)chemical activities for both H_2 production and photocurrent generation (through the methyl viologen redox couple in the suspension), compared to colloidal TiO_2 and commercial TiO_2 nanoparticles (P25 and Hombikat UV-100). The higher photocatalytic activity of meso-TiO_2 is attributed to the compact packing of TiO_2 nanoparticles forming uniform agglomerates, which enable the efficient charge separation through the interparticle CT.

TiO_2 fibers consisting of nanoparticles represent another good example of effective interparticle CT. It is well known that electrospinning of pre-crystallized TiO_2 nanoparticles creates well-ordered and aligned high surface area mesoporous TiO_2 nanofibers that are ~500 nm in diameter and a few micrometers in length (Fig. 9b).[163] Photocatalytic activity comparison between the titania nanofibers (TNF) and the nanoparticles (TNP) indicated that the former had 3 times higher activities in photocurrent generation and 7 times higher in H_2 production. The photocatalytic superiority of TNF is attributed to the effects of mesoporosity and nanoparticle alignment, which help efficient charge separation through interparticle CT along the nanofiber framework. The TNF also exhibited 7 times and >140 times higher dye-sensitized H_2 production, compared to the TNP and commercial TiO_2 samples, respectively.[166] These studies, therefore, provide strong evidence that the charge separation efficiency could be markedly enhanced through interparticle CTs when the individual nanoparticles are directionally arranged with close contacts among them.

3.2. Multi-hybrid semiconductor systems with heterojunction

Combining two different types of semiconductor particles with heterojunction has been frequently employed as a mean of enhancing charge pair separation and thereby enhancing the overall photocatalytic activity.[25,167] A proper selection of semiconductors based on their CB and VB positions leads to the cascaded transfer of photogenerated charge carriers from one semiconductor to another. A variety of binary composites consisting of TiO_2 and other semiconductors (e.g., WO_3,[26,84,168-170] SnO_2,[171-173] ZrO_2,[173] CdSe,[174,175] CdS[25,32,176,177]) have been prepared and tested for their photocatalytic activities.

Among the binary TiO_2 composites with heterojunction, WO_3/TiO_2 composite photocatalysts have been most frequently studied for environmental remediation and solar energy storage.[26,168-170,178-181] The primary role of WO_3 is to accept TiO_2 CB electron. Since WO_3 has a lower (more positive) CB potential than the TiO_2 CB, the TiO_2 CB electrons are transferred to the WO_3 CB with reducing W(VI) to W(V). The reduced state of WO_3 (e.g., as a form of H_xWO_3) is maintained for a period of time and the stored electrons are slowly released to the surrounding electron acceptors (e.g., O_2) (Fig. 10a).[26,182,183] This photocharge-discharge mechanism has been applied to the corrosion prevention of metals by coating the metal surface with the composite semiconductors. This mechanism was also successfully applied to the conversion of water pollutants (phenol, Cr(VI), etc).[26,168] The coupling TiO_2 with WO_3 decreased the photocatalytic activities in some cases (e.g., for the gas-phase oxidation of acetaldehyde and the liquid-phase oxidation of 2-naphthol),[178] In addition, the PCO activity of WO_3/TiO_2 for 1,4-dichlrobenzene was shown to be highest only at a certain ratio of WO_3 to TiO_2 and higher loadings of WO_3 above this fraction decreased the activity significantly.[181] The reduced activity is ascribed to a retarded rate of electron transfer from the WO_3 CB (0.3 – 0.5 V_{NHE}) to O_2, since its potential is more positive than the O_2 reduction potential ($E^\circ(O_2/O_2^{-\bullet})$ = –0.33 V_{NHE}). This problem can be overcome by loading Pt nanoparticles on WO_3, which enables the multi-electron reduction of O_2, which has more positive potential (e.g., $E^\circ(O_2/H_2O_2)$ = +0.695 V_{NHE} for two-electron reduction) than the one-electron reduction.[184] Consequently, the PCO reactions occurring on Pt/WO_3 was markedly enhanced because the reductive decomposition of H_2O_2 (in situ generated from the reduction of O_2) produced OH radicals under visible light.[23]

On the other hand, the mismatch of the CB and VB levels in coupling semiconductor systems may reduce their photocatalytic and PEC activities on the contrary. The hybridization of hematite (α-Fe_2O_3) on TiO_2 nanotube arrays unexpectedly decreased PEC and photocatalytic activity (for phenol degradation), primarily due to the low conductivity of hematite and the band position mismatch between TiO_2 and hematite (the CB and VB of hematite being more positive and negative, respectively, with respect to those of TiO_2).[164] Such mismatch results in enhanced charge recombination.

As for the TiO_2 hybrid with non-oxide semiconductors, CdS/TiO_2 is the most representative example and has been widely applied to the photocatalytic conversion of various substrates such as methane,[185] methyl orange,[186] indole,[187] acid orange II,[188] 1,2,3,4-tetrachlorobenzene,[189] and methylene blue and eosin.[190] The VB and CB of CdS are ideally placed in comparison to those of TiO_2 for efficient charge pair separation and the bandgap of CdS is narrow (~2.5 eV) enough to absorb a substantial portion of solar visible light ($\lambda \leq 500$ nm). Upon excitation by visible light, the CdS CB electrons are transferred to the TiO_2 CB, while the holes remain in the CdS VB (Fig. 10b). Under optimal conditions, the semiconductor coupling reduces the average emission lifetime of CdS by a factor of four (24.6 to 6.8 ns), owing to the scavenging of the CB electrons by TiO_2.[191] The electron transfer from CdS to TiO_2 is sensitively influenced by the CB edge potential difference. As the CdS particle size decreases to the quantum confinement domain, the bandgap of CdS is widened. As a result, the CB edge of CdS rises with respect to that of TiO_2, which increases the driving force of CB electron transfer from CdS to TiO_2.[192,193]

The CdS/TiO_2 composite can be further modified by noble metal (Pt) nanoparticles. In this ternary configuration (i.e., CdS, TiO_2, and noble metal), both semiconductors can be simultaneously excited at different wavelength regions (λ_{TiO2} < 400 nm; λ_{CdS} > 400 nm) due to their different bandgaps. Upon excitation of both CdS and TiO_2, CB electrons and VB holes are separated to TiO_2 and CdS, respectively, while electrons are effectively collected at metal nanoparticles (Pt) deposited on TiO_2 (Fig. 10c). This CT process mimics that of natural photosynthesis[194] in terms of two-photon excitation (PS-II and PS-I in Z-scheme: *see* Fig. 5a). It is important that Pt is loaded selectively on TiO_2 surface only among the CdS/TiO_2 composite since the electrons are transferred to the TiO_2 side. For example, the photoplatinized hybrid of CdS/TiO_2 [resulting in Pt-(CdS/TiO_2) where Pt are loaded on both CdS and TiO_2] is much less efficient than the hybrid of CdS/(Pt-TiO_2) [Pt photodeposited on TiO_2 first then followed by the deposition of CdS]. The CdS/(Pt-TiO_2) exhibits 3 – 30 fold higher H_2 production compared to Pt-(CdS/TiO_2).[32]

Another ideal candidate for non-oxide semiconductor coupled with TiO_2 is TaON. The narrow bandgap of TaON (~ 2.4 eV),[195] along with the negatively shifted CB and VB edges compared to those of TiO_2, induces efficient charge separation at the TiO_2/TaON interface. Nevertheless, there have not been many studies on the coupling of TaON and TiO_2, owing to the harsh synthesis conditions of TaON. The synthesis of TaON generally requires high temperature nitridation (at over 850 ^oC),[196] which induces particle coarsening and phase transformation of the counter semiconductor (e.g., the transformation of TiO_2 to TiN).[21,197,198] Recently, TaO_xN_y thin layer coupled with TiO_2 nanotubes (TNTs) was prepared by a low temperature nitridation process (500 ^oC) and

the TNT composite exhibited much improved PEC water-splitting efficiencies under both visible (3.6 times) and UV (1.8 times) illumination compared to bare TNTs because of the efficient charge pair separation at the heterojunction interface of TaO_xN_y/TNTs (Fig. 11).[199] In addition, the thin TaO_xN_y layer on TNTs serves as a passivation layer that reduces the surface trap sites and enhances the visible light absorption range.

Ternary hybrid systems have received less attention because of the complexity while the binary systems have been extensively studied. To evaluate the effects of the ternary systems, a systematic study was conducted with CdS/TiO_2/WO_3 hybrids, which have cascadal positioning of the CB edges (*see* Fig. 10d). In this study, only CdS was selectively excited under the irradiation of $\lambda > 495$ nm (equivalent to 2.51 eV), in order to focus on the cascaded electron transfer starting from CdS in the ternary hybrid. The photocatalytic reduction of polyoxometallate (POM) ($E°(PMo_{12}O_{40}^{3-/4-}) = +0.65\ V_{NHE}$) and PEC tests indicated that the CdS/TiO_2/WO_3 ternary hybrid has much higher activities compared to bare CdS and binary hybrids (CdS/TiO_2 or CdS/WO_3) because of the cascadal electron transfer through two sequential heterojunctions (CdS → TiO_2 → WO_3). Unlike the binary system where the separated charge pairs may recombine directly at the heterojunction, the two sequential heterojunctions along the potential gradient reduces the chance of direct recombination of charge carriers because the electron can be further transferred to the third compartment. The presence of TiO_2 in between CdS and WO_3 provides an energy barrier for the back electron transfer (Fig. 10d). However, the cascadal electron transfer from CdS to TiO_2 to WO_3 reduces the reduction potential of CB electrons progressively, which limits the range of reductive

conversions that can be driven by the ternary hybrid photocatalytic system. For example, when tungstosilicate ($SiW_{12}O_{40}^{4-}$), which has more negative one-electron reduction potential ($E° = +0.054\ V_{NHE}$) compared to WO_3 CB, was used as an alternative POM, the efficiency of the photocatalytic reduction was markedly diminished. The cost of enhancing the charge separation efficiency in the hybrid structure is to make the electrons less energetic.

4. Visible light-induced charge transfers

Visible light sensitization of wide bandgap semiconductors like TiO_2 has been intensively investigated as one of the most important research topics in photocatalysis. Unlike the heterojunction semiconductors and impurity-doped semiconductors which are modified primarily by inorganic components, the visible light sensitization of semiconductors can be also achieved by coupling with organic substances. There are two main methods for achieving visible light-induced CT: dye-sensitization[166,200,201] and ligand-to-metal charge transfer (LMCT).[202-211]

4.1. Dye sensitization

Dye-sensitization of semiconductor photocatalysts is conceptually similar to the operation mechanism of dye-sensitized solar cells.[15,212] In principle, dye molecules located at the TiO_2/solution interface are photoexcited and subsequently inject electrons into the TiO_2 CB (Fig. 12a). These electrons are subsequently transferred to electron acceptors to induce various redox reactions at the semiconductor interface. For effective electron injection from the excited dye to TiO_2, it is necessary to firmly anchor the dye

molecules onto the TiO_2 surface. In aqueous environments, the adsorption of dyes usually proceeds via electrostatic interaction with the amphoteric TiO_2 surface (>Ti-$OH_2^+ \leftrightarrow$ >Ti-OH $\leftrightarrow$ >Ti-O^-),[4,8] the surface charge of which depends on the solution pH. For example, the most commonly used ruthenium bipyridyl complexes (Ru-bpy) with carboxylate anchoring groups are readily anchored to the TiO_2 surface in acidic pH region,[97,98,213-215] because the point of zero charge of TiO_2 is around pH_{zpc} ~ 6 (Fig. 12b).[4,8,75] At pH < 6, the surface of TiO_2 is positively charged and attracts the carboxylate anion anchoring groups and the dye anchoring is efficiently achieved. The sensitization of anchored dyes can successfully induces H_2 evolution[201,214,215] and the conversion of water pollutants *(e.g.,* dechlorination of CCl_4, reduction of Cr^{6+}) under visible light.[97,200,201] However, at pH > 6 where the TiO_2 surface is negatively charged, the anionic dyes are electrostatically repelled and the sensitization efficiency decreases.[200,201,213,214] Organic dyes with carboxylate groups also show similar behaviors.[200,201] To widen the working pH range, the carboxylate anchoring group can be replaced with phosphonate group.[213,216] TiO_2 sensitized with Ru-bpy containing phosphonate groups shows activity for H_2 evolution even at alkaline pH (~9). The number of anchoring groups (carboxylates vs. phosphonates) also significantly influences the photoefficiency and stability of dye-sensitized TiO_2 systems.[213,216] Irrespective of the kind and number of anchoring groups, the pre-adsorption of dyes on TiO_2 is usually required for the initiation of the sensitization.

Interestingly, some studies have shown that the presence of pre-adsorbed dye is not always necessary for dye sensitization in aqueous environments. One example is the tin(IV)-porphyrin (SnP)-sensitized TiO_2 system (Fig. 12c).[217] SnP has a strong oxidative

power due to the high charge on Sn(IV)[218,219] and hence the excited SnP shows a high photoactivity for the oxidation of aqueous organic compounds. Although the adsorption of SnP on TiO_2 is negligible in the pH range of 3 ~ 11, a significant amount of H_2 was produced in the SnP/TiO_2 system (turnover number of 410 and quantum efficiency of ~35% at an irradiation wavelength of 550 nm).[217] Laser flash photolysis showed that the free excited SnP is first reduced by an electron donor (e.g., EDTA) owing to its strong oxidation power in the nanosecond time scale. The high charge on Sn(IV) makes the SnP ring highly electrophilic, favoring the formation of the SnP π-radical anion ($SnP^{\bullet -}$). The lifetime of the π-radical anion is long enough (in the order of microseconds) to survive during the slow diffusion from the solution bulk to the TiO_2 surface. As a result, the adsorption of SnP on TiO_2 is not a required condition for H_2 production. This is in contrast with the case of the Ru-bpy/TiO_2 system, where the electron transfer from the electron donor to Ru-bpy is 6-9 orders of magnitude slower than the electron injection from the excited Ru-bpy to TiO_2.

4.2. Ligand-to-metal charge transfer (LMCT) sensitization

An alternative modification method for visible light activation of TiO_2 is to form CT complexes between TiO_2 and the surface adsorbate (ligand), neither of which absorbs visible light.[210,220,221] This CT-complex-mediated visible light sensitization operates by a mechanism that is different from the aforementioned dye sensitization. In the CT-sensitization, the electron is photoexcited directly from the ground state (HOMO level) of the adsorbate (ligand) (without involving the excited state of the adsorbate) to the semiconductor CB with mainly metal orbital characters (so named as *ligand-to-metal charge transfer*, LMCT) (Fig. 13a), whereas the dye sensitization is mediated through

the excited dye state. Many examples of CT-complex formation on the TiO_2 surface have been reported. TiO_2–catechol complex is a classical example of CT-complexation. A theoretical calculation study provided evidence that the visible light absorption is caused by the LMCT and the excited state of catechol is not significantly involved in the photoinjection process.[208] 8-hydroxyorthoquinoline and 1,1-binaphthalene-2,2-diol also form complexes with the TiO_2 surface, absorbing visible light and exhibiting some activity for H_2 production under visible light.[202,203] Many organic compounds with phenolic or carboxylic groups (e.g., chlorophenol,[205] calixarene[206]) are able to make LMCT-complexes with the TiO_2 surface for visible light absorption. Upon coupling with TiO_2, the relatively electron-rich compounds with linker groups (e.g., enediol, carboxylate, nitrile, and alcohol) exhibit a LMCT band in the visible region, whereas the less electron-rich compound (e.g., thiocyanate) display the band in the UV region.[209] The HOMO level of the adsorbate is also very important in determining the active light absorption range of the LMCT system. If there is strong coupling between the molecular orbital (HOMO) of the adsorbate and energy band of the semiconductor, a new absorption band could appear that is absent in either the adsorbate or semiconductor alone. Incidentally, the fact that pure TiO_2 sometimes exhibits visible light activity for the degradation of organic substrates that do not absorb visible light at all can be ascribed to the LMCT mechanism. For example, phenol and 4-CP can be successfully degraded with producing chloride ions or/and CO_2 in visible light illuminated ($\lambda > 420$ nm) aqueous suspension of pure TiO_2 although neither TiO_2 nor phenolic compounds absorb visible light.[205] This is because the phenolic compound adsorbed on TiO_2 (though very weakly) can inject an electron to TiO_2 CB through LMCT with oxidizing itself.

LMCT sensitization with relatively cheap and commonly used compounds is also noteworthy. For example, ethylenediaminetetraacetate (EDTA) and formate that are widely utilized as an electron donor in photochemical conversion systems can induce the LMCT-sensitization by forming surface complexes. The complexation of EDTA (or formate) on TiO_2 induces visible light absorption up to ~550 nm and exhibits a significant visible light activity for both the reductive conversion of Cr(VI) → Cr(III) and the production of H_2 from water.[204] Glucose that is also commonly employed as an electron donor in photocatalysis can also form a LMCT complex on TiO_2 surface.[222] The TiO_2-glucose LMCT complex absorbs visible light significantly (up to 600 nm) and exhibits visible light activity for the photoconversion of Cr(VI) to Cr(III) and the production of H_2O_2 via O_2 reduction. Hydrogen peroxide (H_2O_2) that is widely employed as an auxiliary oxidant in TiO_2/UV process can also form an LMCT complex on TiO_2 surface but it is unstable and rapidly decomposes under visible light with generating an OH radical.[84] Although most LMCT sensitization systems are based on the chemisorbed adsorbates, LMCT sensitization phenomenon can be observed even with physisorbed adsorbates in some cases. For instance, pure polycyclic arenes (chrysene, anthracene, pyrene and benzo[a]pyrene) can form LMCT complexes with dry surface of TiO_2 (absent of adsorbed water molecules) and the resulting colored arene–TiO_2 complex could be reversibly bleached by desorbing the arenes without degrading the arene compounds.[85] A physical mixture of TiO_2 and non-ionic surfactants with polyoxyethylene groups (Brij series) that do not absorb visible light at all by themselves is another example of physisorbed LMCT.[223] The suspension of surfactant/TiO_2 showed a weak and broad absorption band in the visible light region (320 – 500 nm) and the visible light-induced electron transfer initiated on surfactant/TiO_2 reductively

transformed CCl_4 into Cl^- and CO_2 or Cr(VI) to Cr(III). Considering the above examples, it seems that the visible light induced charge transfer occurring directly between the surface adsorbate and semiconductor is quite ubiquitous as long as the HOMO level of the adsorbate lies below the CB edge level. However, the degree of the charge transfer interaction is usually very weak and often negligible unless the interfacial orbital coupling is strong.

The LMCT sensitization phenomenon can be actively employed as a basis of the development of visible light active photocatalysts. For example, a linear-structured novolac type phenolic resin (PR) was shown to be successfully grafted onto the TiO_2 surface by simply dispersing the PR and TiO_2 powders in acetone (Fig. 13b).[211] The PR/TiO_2 exhibited yellowish and brownish color (depending on the PR loading) and was found to be active for the evolution of H_2 from water and the degradation of 4-CP under visible light (λ > 420 nm). The direct HOMO(-6.6 eV)-LUMO(-3.1 eV) excitation of PR requires 3.5 eV, which cannot be induced by visible light, but the LMCT between the PR HOMO and the TiO_2 CB is enabled by visible light photons of ca. 2.2. eV (< 560 nm). The PR as a sensitizer of TiO_2 has the following advantages: (1) the synthesis process is easy, fast, and mild, (2) it is insoluble and stable in water, (3) it rapidly forms a surface complex without the need of additional linkage groups, and (4) it is much cheaper than organometallic dye sensitizers. Another LMCT-type visible light photocatalyst was developed by anchoring fullerol ($C_{60}(OH)_x$) on the surface of TiO_2 (Fig. 13c).[207] In contrast to fullerene (C_{60}), fullerol adsorbs well on TiO_2 at pH 3 via monodentate and/or multidentate hydroxyl group complexation. The adsorbed fullerol activates the TiO_2 under visible light irradiation through the CT-sensitization

mechanism, which is insignificant in the fullerene/TiO_2 system. Fullerol/TiO_2 exhibits significant visible photocatalytic activity for not only the redox conversion of organic and inorganic substrates (4-CP, I^-, and Cr(VI)) but also H_2 evolution from water. The surface complexation of fullerol/TiO_2 induces a visible absorption band around 400–500 nm, which is extinguished when the adsorption of fullerol is inhibited. Transient absorption spectroscopic measurements revealed an absorption spectrum ascribed to fullerol radical cation (fullerol$^{\bullet+}$), the generation of which should be accompanied by the proposed CT. Theoretical calculations regarding the absorption spectra for the "TiO_2 cluster + fullerol" model also confirmed the proposed CT, which involves the excitation from HOMO (fullerol) to LUMO (TiO_2 cluster) as the origin of the visible-light absorption of Fullerol/TiO_2.

5. Dual purpose photocatalysis for simultaneous energy and environmental applications

The photocatalytic conversion processes are carried out under different experimental conditions depending on their applications. The photocatalysis for the degradation of pollutants is initiated by the single electron transfer resulting in the generation of reactive radical species and therefore this process is usually carried out in the presence of dissolved O_2 (aerated condition). The dioxygen is needed not only as an electron acceptor that scavenges the CB electrons but also as a precursor of ROS and a reactant for mineralization.[96,126,127,224] Therefore, the photocatalytic degradation and mineralization of organic substrates does not proceed in the absence of O_2. On the other

hand, the photocatalysis for solar fuel synthesis such as H_2 production is mediated by multi-electron transfer process and is carried out in the absence of O_2 (anoxic condition), the presence of which should compete with H_2O (or protons) for CB electrons and reoxidize H_2 back to water. The presence of dioxygen hinders the photocatalytic production of H_2. Therefore, the two photocatalytic systems have been practiced separately under different reaction conditions and any photocatalyst may not be optimized for both purposes. A good photocatalyst for the environmental cleanup may be poor for solar fuel synthesis while an excellent photocatalyst for water splitting may be poor for environmental remediation purpose. It is quite challenging to achieve the two purposes in a single system of "dual-functional photocatalysis" (*e.g.,* simultaneous production of H_2 and the degradation of pollutants in wastewater). To achieve this, photocatalysts should be able to oxidize organic substrates with utilizing proton or water (not O_2) as an electron acceptor while producing hydrogen at the same time. The successful development of this concept would realize the photocatalytic water treatment that removes unwanted organic pollutants and recovers H_2 as an energy resource at the same time. Although this system is conceptually identical to widely investigated sacrificial photocatalytic systems for H_2 production, which employ excess amounts of good electron donors (e.g., organic acids, alcohols, and sulfides/sulfites),[225-228] the challenge lies in the development of photocatalysts that can utilize low concentration organic contaminants as an electron donor for H_2 production. If organic pollutants can be used as an electron donor for H_2 production, the overall photocatalytic process can be cost-effective. The development of photocatalytic systems that combine wastewater treatment and H_2 production is promising because a variety of organic pollutants found in wastewaters may serve as precursors for H_2 in solar photocatalysis.

Many electrochemical and PEC studies have investigated the simultaneous production of energy (e.g., H_2 and electricity) and the degradation of organic pollutants (e.g., phenolic compounds, dyes, organic acids, actual wastewater, and urea/urine).[229-234] They have used either external electrical energy or photovoltaics (Fig. 14a). Conceptually, the dual functional process occurring on (suspended) TiO_2 particles is similar to the case of (photo)electrochemical system. However, since external electric power cannot be applied to the slurry system, the efficiency of the charge pair separation in a single TiO_2 particle is low.[235] The functional photocatalysis usually needs the presence of co-catalysts (e.g., Pt for hydrogen evolution reaction and RuO_2 for oxygen evolution reaction) that are deposited on the TiO_2 surface.[236]

Recently, TiO_2 of which surface is modified with both fluoride (or phosphate) and platinum nanoparticle (F-TiO_2/Pt or P-TiO_2/Pt) has been successfully demonstrated for the dual function photocatalysis: simultaneous degradation of organic compounds and H_2 production under a solar simulating condition ($\lambda > 320$ nm) (Fig. 14b).[76,79,80] Surface fluorination (or phosphation) replaces the surface hydroxyl groups on TiO_2, favoring the formation of unbound OH radicals ($\bullet OH_f$) instead of surface-bound OH radicals (>Ti-OH$\bullet$) (Fig. 14c).[62,65,75,77,78,237] Since the surface-bound OH radicals (or surface-trapped holes) serve as a site of recombination with CB electrons, the fluoride substitution reduces the chance of recombination of CB electron with the surface trapped hole on TiO_2 particles. Meanwhile, surface platinization accelerates the electron transfer and further retards the charge pair recombination, thereby enhancing H_2 production significantly.[23,32,37,85,99,114,238] With these catalysts, the degradation of 4-CP and urea can be accompanied by the concurrent production of H_2 (Fig. 14b). The synergistic effect greatly depends on the type of metal (Pt, Pd, Au, Ag, Cu, or Ni) and

pH. The activity of F-TiO_2/Pt gradually decreases with increasing pH, owing to the desorption of fluoride from the TiO_2 surface. On the other hand, P-TiO_2/Pt maintains the activity over a wide pH range because of the stability of adsorbed phosphate, making the catalyst a more practical dual-function photocatalyst. Recently, the F-TiO_2/Pt catalyst was further modified by the third component, graphene oxide (GO) to enhance the dual-functional photocatalytic activity.[239] GO on TiO_2 attracts electrons and facilitates the electron transfer to Pt. The positive effect of GO on the dual photocatalytic activity was observed only when Pt and surface fluoride are co-present. The photocatalytic activity of Pt/GO/TiO_2-F (ternary system) for the simultaneous H_2 production accompanied with the degradation of 4-CP was much higher than any of binary-component photocatalysts, which confirmed the synergic role of the three components (*i.e.,* GO, Pt, F).

6. Concluding remarks

Most semiconductor metal oxides including titania have limited photoactivity because of rapid charge recombination. Surface modification of semiconductor photocatalysts is a facile and soft method without reconstructing the solid lattice structure and has been widely attempted to improve the photocatalytic activity under UV and/or visible light irradiation. The modified surface of semiconductor critically influences the photo-induced CT behaviors at the interfacial region (particle/solution, particle/air, and particle/particle). Therefore, it is essential to understand how the modified surface properties control the primary factors involved in the overall photocatalysis. The photogenerated charge carriers follow various pathways which include recombination,

trapping (at surface and bulk defect sites), transfer to a reservoir phase (*e.g.,* Pt, graphene), transfer to a bordering particle (of the same or different kind), and transfer to electron acceptor/donor in the electrolyte. For desirable photocatalytic reactions, the eventual transfer to electron acceptors or donors (i.e., target substrate) should be maximized, which can be controlled by modifying the surface properties. The effects of a specific modification method depends on many parameters and are specific to the kind of substrates, the characteristics of target reactions, and the experimental conditions. For example, a modified semiconductor optimized for a single-CT may not be good for a multiple-CT system (and *vice versa*). Therefore, it is usually not possible to generalize the effects of a specific modification method: even the same modified semiconductor may exhibit either a positive or a negative effect depending on the nature of the target photocatalytic conversion system. This implies that finding out "the best modification method" out of numerous possible ways of semiconductor modifications is not very meaningful. Each modification method and its related effects can be clearly defined only for a specific photocatalytic system. For example, it is not difficult to find out the published articles which claim that they developed a very efficient photocatalyst (hybrid or modified) based on a dye-discoloration measurement with an assumption that the particular photocatalyst would be also good for other photocatalytic conversion systems in general, which is actually not. The result could be different for other photocatalytic systems and even for a different dye.[240] Therefore, the modification method of semiconductor photocatalysts should be cautiously chosen or designed on the basis of clear understanding on the characteristics of the target reaction. The dual-function photocatalysis, for example, aims to achieve the single CT for the pollutant oxidation part but the multiple-CT for H_2 production part on the contrary, which is to control the

transfer of holes and electrons in semiconductor particles in different ways. The development of proper modification methods to selectively control the CT behavior may realize such goal.

Acknowledgements

This research was financially supported by the Global Research Laboratory (GRL) Program (No. NRF-2014K1A1A2041044), the Global Frontier R&D Program on Center for Multiscale Energy System (2011-0031571), and KCAP (Sogang Univ.) (No. 2009-0093880), which were funded by the Korea Government (MSIP) through the National Research Foundation (NRF). H.P. is grateful to Global Research Network Program (NRF-2014S1A2A2027802) for financial support.

References

1 N. Serpone and E. Pelizzetti, *Photocatalysis: Fundamentals and Applications*, Wiley, New York, 1989.
2 C. A. Grimes, O. K. Varghese and S. Ranjan, *Light, Water, Hydrogen: The Solar Generation of Hydrogen by Water Photoelectrolysis*, Springer, New York, 2008.
3 R. Van de Krol and M. Gratzel, *Photoelectrochemical Hydrogen Production*, Springer, New York, 2012.
4 M. R. Hoffmann, S. T. Martin, W. Choi and D. W. Bahnemann, *Chem. Rev.*, 1995, **95**, 69-96.
5 A. Fujishima, X. T. Zhang and D. A. Tryk, *Surf. Sci. Rep.*, 2008, **63**, 515-582.
6 M. J. Esswein and D. G. Nocera, *Chem. Rev.*, 2007, **107**, 4022-4047.
7 W. Choi, *Catal. Surv. Asia*, 2006, **10**, 16-28.
8 H. Park, Y. Park, Y. Kim and W. Choi, *J. Photochem. Photobiol., C*, 2012, **15**, 1-20.
9 L. Vayssieres, ed., *On Solar Hydrogen & Nanotechnology*, Wiley, Singapore, 2009.
10 J. Lee, J. Kim and W. Choi, in *Aquatic Redox Chemistry*, eds. P. G. Tratnyek, T. J. Grundl and S. B. Haderlein, American Chemical Society, Washington, 2011.
11 S. Licht, in *Encyclopedia of Electrochemistry*, eds. A. J. Bard and M. Stratmann, Wiley-VCH, Weinheim, 2002.
12 N. Serpone, *J. Phys. Chem. B*, 2006, **110**, 24287-24293.
13 P. V. Kamat, *J. Phys. Chem. B*, 2002, **106**, 7729-7744.
14 T. L. Thompson and J. T. Yates, Jr., *J. Phys. Chem. B*, 2005, **109**, 18230-18236.
15 G. Hodes, *J. Phys. Chem. C*, 2008, **112**, 17778-17787.
16 T. Tachikawa, M. Fujitsuka and T. Majima, *J. Phys. Chem. C*, 2007, **111**, 5259-5275.
17 K. Maeda and K. Domen, *J. Phys. Chem. Lett.*, 2010, **1**, 2655-2661.
18 J. A. Turner, *Science*, 1999, **285**, 687-689.
19 U. Kang and H. Park, *Appl. Catal., B*, 2013, **140-141**, 233-240.
20 T. H. Jeon, S. K. Choi, H. W. Jeong, S. Kim and H. Park, *J. Electrochem. Sci. Technol.*, 2011, **2**, 187-192.
21 M. Tabata, K. Maeda, M. Higashi, D. L. Lu, T. Takata, R. Abe and K. Domen, *Langmuir*, 2010, **26**, 9161-9165.
22 H. W. Jeong, S.-Y. Choi, S. H. Hong, S. K. Lim, D. S. Han, A. Abdel-Wahab and H. Park, *J. Phys. Chem. C*, 2014, **118**, 21331-21338.
23 J. Kim, C. W. Lee and W. Choi, *Environ. Sci. Technol.*, 2010, **44**, 6849-6854.
24 J. Kim and W. Choi, *Environ. Sci. Technol.*, 2011, **45**, 3183-3184.
25 H.-i. Kim, J. Kim, W. Kim and W. Choi, *J. Phys. Chem. C*, 2011, **115**, 9797-9805.
26 H. Park, A. Bak, T. H. Jeon, S. Kim and W. Choi, *Appl. Catal., B*, 2012, **115-116**, 74-80.
27 C. Tagusagawa, A. Takagaki, A. Iguchi, K. Takanabe, J. N. Kondo, K. Ebitani, T. Tatsumi and K. Domen, *Chem. Mater.*, 2010, **22**, 3072-3078.
28 A. Bak, W. Choi and H. Park, *Appl. Catal., B*, 2011, **110**, 207-215.
29 T. H. Jeon, W. Choi and H. Park, *Phys. Chem. Chem. Phys.*, 2011, **13**, 21392-21401.
30 M. Yoshida, T. Hirai, K. Maeda, N. Saito, J. Kubota, H. Kobayashi, Y. Inoue and K. Domen, *J. Phys. Chem. C*, 2010, **114**, 15510-15515.
31 D. Yokoyama, T. Minegishi, K. Maeda, M. Katayama, J. Kubota, A. Yamada, M. Konagai and K. Domen, *Electrochem. Commun.*, 2010, **12**, 851-853.
32 H. Park, W. Choi and M. R. Hoffmann, *J. Mater. Chem.*, 2008, **18**, 2379-2385.
33 Y. K. Kim and H. Park, *Energy Environ. Sci.*, 2011, **4**, 685-694.
34 G. Khan, S. K. Choi, S. Kim, S. K. Lim, J. S. Jang and H. Park, *Appl. Catal., B*, 2013, **142-143**, 647-653.
35 Y. Kim and H. Park, *Appl. Catal., B*, 2012, **125**, 530-537.
36 U. Kang, S. K. Choi, D. J. Ham, S. M. Ji, W. Choi, D. S. Han, A. Abdel-Wahab and H. Park, *Energy Environ. Sci.*, 2015, **8**, 2638-2643.
37 H. Park and W. Choi, *J. Phys. Chem. B*, 2003, **107**, 3885-3890.
38 K. Maeda, M. Higashi, D. L. Lu, R. Abe and K. Domen, *J. Am. Chem. Soc.*, 2010, **132**, 5858-5868.
39 J. A. Seabold and K. S. Choi, *Chem. Mater.*, 2011, **23**, 1105-1112.

40 Y. Surendranath, M. Dinca and D. G. Nocera, *J. Am. Chem. Soc.*, 2009, **131**, 2615-2620.
41 S. K. Choi, W. Choi and H. Park, *Phys. Chem. Chem. Phys.*, 2013, **15**, 6499-6507.
42 D. K. Bediako, B. Lassalle-Kaiser, Y. Surendranath, J. Yano, V. K. Yachandra and D. G. Nocera, *J. Am. Chem. Soc.*, 2012, **134**, 6801-6809.
43 C. Tagusagawa, A. Takagaki, K. Takanabe, K. Ebitani, S. Hayashi and K. Domen, *J. Catal.*, 2010, **270**, 206-212.
44 S. J. Li, Z. C. Ma, J. Zhang, Y. S. Wu and Y. M. Gong, *Catal. Today*, 2008, **139**, 109-112.
45 A. Kudo and Y. Miseki, *Chem. Soc. Rev.*, 2009, **38**, 253-278.
46 E. R. Carraway, A. J. Hoffman and M. R. Hoffmann, *Environ. Sci. Technol.*, 1994, **28**, 786-793.
47 C. Richard, *J. Photochem. Photobiol., A*, 1993, **72**, 179-182.
48 Y. Mao, C. Schoneich and K. D. Asmus, *J. Phys. Chem.*, 1991, **95**, 10080-10089.
49 R. B. Draper and M. A. Fox, *Langmuir*, 1990, **6**, 1396-1402.
50 S. Kim and W. Choi, *Environ. Sci. Technol.*, 2002, **36**, 2019-2025.
51 M. C. Lee and W. Choi, *J. Phys. Chem. B*, 2002, **106**, 11818-11822.
52 S. Chen and L.-W. Wang, *Chem. Mater.*, 2012, **24**, 3659-3666.
53 W. Choi, A. Termin and M. R. Hoffmann, *J. Phys. Chem.*, 1994, **98**, 13669-13679.
54 W. Choi, A. Termin and M. R. Hoffmann, *Angew. Chem., Int. Ed.*, 1994, **33**, 1091-1092.
55 M. Mrowetz, W. Balcerski, A. J. Colussi and M. R. Hoffmann, *J. Phys. Chem. B*, 2004, **108**, 17269-17273.
56 S. Kim, S. J. Hwang and W. Choi, *J. Phys. Chem. B*, 2005, **109**, 24260-24267.
57 Y. Park, W. Kim, H. Park, T. Tachikwawa, T. Majima and W. Choi, *Appl. Catal., B*, 2009, **91**, 355-361.
58 W. Kim, T. Tachikawa, H. Kim, N. Lakshminarasimhan, P. Murugan, H. Park, T. Majima and W. Choi, *Appl. Catal., B*, 2014, **147**, 642-650.
59 W. Choi, S. J. Hong, Y. S. Chang and Y. Cho, *Environ. Sci. Technol.*, 2000, **34**, 4810-4815.
60 C. X. Zhang, T. L. Sun and X. M. Sun, *Environ. Sci. Technol.*, 2011, **45**, 4756-4762.
61 H. Park and W. Choi, *J. Phys. Chem. B*, 2005, **109**, 11667-11674.
62 M. S. Vohra, S. Kim and W. Choi, *J. Photochem. Photobiol., A*, 2003, **160**, 55-60.
63 G. Zhang, W. Choi, S. H. Kim and S. B. Hong, *J. Hazard. Mater.*, 2011, **188**, 198-205.
64 P. Chin, C. S. Grant and D. F. Ollis, *Appl. Catal., B*, 2009, **87**, 220-229.
65 J. S. Park and W. Choi, *Langmuir*, 2004, **20**, 11523-11527.
66 H. Haick and Y. Paz, *J. Phys. Chem. B*, 2001, **105**, 3045-3051.
67 S. K. Lee, S. McIntyre and A. Mills, *J. Photochem. Photobiol., A*, 2004, **162**, 203-206.
68 J. S. Park and W. Choi, *Chem. Lett.*, 2005, **34**, 1630-1631.
69 T. Tatsuma, W. Kubo and A. Fujishima, *Langmuir*, 2002, **18**, 9632-9634.
70 T. Tatsuma, S. Tachibana and A. Fujishima, *J. Phys. Chem. B*, 2001, **105**, 6987-6992.
71 T. Tatsuma, S. Tachibana, T. Miwa, D. A. Tryk and A. Fujishima, *J. Phys. Chem. B*, 1999, **103**, 8033-8035.
72 S. M. Cho and W. Choi, *J. Photochem. Photobiol., A*, 2001, **143**, 221-228.
73 P. Chin, G. W. Roberts and D. F. Ollis, *Ind. Eng. Chem. Res.*, 2007, **46**, 7598-7604.
74 W. Kim, T. Tachikawa, G. Moon, T. Majima and W. Choi, *Angew. Chem., Int. Ed.*, 2014, **53**, 14036-14041.
75 H. Park and W. Choi, *J. Phys. Chem. B*, 2004, **108**, 4086-4093.
76 J. Kim and W. Choi, *Appl. Catal., B*, 2011, **106**, 39-45.
77 H. Kim and W. Choi, *Appl. Catal., B*, 2006, **69**, 127-132.
78 J. Kim, W. Choi and H. Park, *Res. Chem. Intermed.*, 2010, **36**, 127-140.
79 J. Kim, J. Lee and W. Choi, *Chem. Commun.*, 2008, 756-758.
80 J. Kim, D. Monllor-Satoca and W. Choi, *Energy Environ. Sci.*, 2012, **5**, 7647-7656.
81 C. Minero, G. Mariella, V. Maurino and E. Pelizzetti, *Langmuir*, 2000, **16**, 2632-2641.
82 V. Maurino, C. Minero, G. Mariella and E. Pelizzetti, *Chem. Commun.*, 2005, 2627-2629.
83 M. Mrowetz and E. Selli, *Phys. Chem. Chem. Phys.*, 2005, **7**, 1100-1102.
84 T. Ohno, F. Tanigawa, K. Fujihara, S. Izumi and M. Matsumura, *J. Photochem. Photobiol., A*, 1998, **118**, 41-44.
85 H. Park, J. Lee and W. Choi, *Catal. Today*, 2006, **111**, 259-265.
86 R. Abe, M. Higashi and K. Domen, *J. Am. Chem. Soc.*, 2010, **132**, 11828-11829.
87 S. S. K. Ma, T. Hisatomi, K. Maeda, Y. Moriya and K. Domen, *J. Am. Chem. Soc.*, 2012, **134**, 19993-19996.

88 H. Kim, H.-Y. Yoo, S. Hong, S. Lee, B.-S. Park, H. Park, C. Lee and J. Lee, *Appl. Catal., B.*, 2015, **162**, 515-523.
89 D. F. Evans and M. W. Upton, *J. Chem. Soc., Dalton Trans.*, 1985, 1141-1145.
90 S. T. Martin, A. T. Lee and M. R. Hoffmann, *Environ. Sci. Technol.*, 1995, **29**, 2567-2573.
91 E. Pelizzetti, V. Carlin, C. Minero and M. Gratzel, *New J. Chem.*, 1991, **15**, 351-359.
92 W. V. Steele and E. H. Appelman, *J. Chem. Thermodyn.*, 1982, **14**, 337-344.
93 R. R. Ozer and J. L. Ferry, *Environ. Sci. Technol.*, 2001, **35**, 3242-3246.
94 I. A. Weinstock, *Chem. Rev.*, 1998, **98**, 113-170.
95 J. Lee, J. Kim and W. Choi, *Environ. Sci. Technol.*, 2007, **41**, 3335-3340.
96 J. Ryu and W. Choi, *Environ. Sci. Technol.*, 2006, **40**, 7034-7039.
97 Y. Cho, W. Choi, C. H. Lee, T. Hyeon and H. I. Lee, *Environ. Sci. Technol.*, 2001, **35**, 966-970.
98 E. Bae and W. Choi, *Environ. Sci. Technol.*, 2002, **37**, 147-152.
99 S. Kim and W. Choi, *J. Phys. Chem. B*, 2002, **106**, 13311-13317.
100 C. D. Vecitis, H. Park, J. Cheng, B. T. Mader and M. R. Hoffmann, *Front. Environ. Sci. Eng.*, 2009, **3**, 129-151.
101 H. Park, C. D. Vecitis, J. Cheng, W. Choi, B. T. Mader and M. R. Hoffmann, *J. Phys. Chem. A*, 2009, **113**, 690-696.
102 E. Szajdzinska-Pietek and J. L. Gebicki, *Res. Chem. Intermed.*, 2000, **26**, 897-912.
103 H. Park, C. D. Vecitis, J. Cheng, N. F. Dalleska, B. T. Mader and M. R. Hoffmann, *Photochem. Photobiol. Sci.*, 2011, **10**, 1945-1953.
104 H. Kyung, J. Lee and W. Choi, *Environ. Sci. Technol.*, 2005, **39**, 2376-2382.
105 S. Kim and H. Park, *RSC Adv.*, 2013, **3**, 17551-17558.
106 W. Choi and M. R. Hoffmann, *Environ. Sci. Technol.*, 1995, **29**, 1646-1654.
107 W. Choi and M. R. Hoffmann, *Environ. Sci. Technol.*, 1997, **31**, 89-95.
108 B. Kraeutler and A. J. Bard, *J. Am. Chem. Soc.*, 1978, **100**, 4317-4318.
109 M. Jakob, H. Levanon and P. V. Kamat, *Nano Lett.*, 2003, **3**, 353-358.
110 W. Choi, J. Lee, S. Kim, S. Hwang, M. C. Lee and T. K. Lee, *J. Ind. Eng. Chem.*, 2003, **9**, 96-101.
111 J. Lee, W. Choi and J. Yoon, *Environ. Sci. Technol.*, 2005, **39**, 6800-6807.
112 I. Mikami, S. Aoki and Y. Miura, *Chem. Lett.*, 2010, **39**, 704-705.
113 L. A. Pretzer, P. J. Carlson and J. E. Boyd, *J. Photochem. Photobiol., A*, 2008, **200**, 246-253.
114 J. Lee and W. Choi, *Environ. Sci. Technol.*, 2004, **38**, 4026-4033.
115 J. Lee and W. Choi, *J. Phys. Chem. B*, 2005, **109**, 7399-7406.
116 J. Lee, H. Park and W. Choi, *Environ. Sci. Technol.*, 2002, **36**, 5462-5468.
117 W. Zhao, C. Chen, X. Li, J. Zhao, H. Hidaka and N. Serpone, *J. Phys. Chem. B*, 2002, **106**, 5022-5028.
118 N. Z. Muradov, *Sol. Energy*, 1994, **52**, 283-288.
119 D. Hufschmidt, D. Bahnemann, J. J. Testa, C. A. Emilio and M. I. Litter, *J. Photochem. Photobiol., A*, 2002, **148**, 223-231.
120 B. Sun, V. Vorontsov and P. G. Smirniotis, *Langmuir*, 2003, **19**, 3151-3156.
121 M. Trillas, J. Peral and X. Domenech, *Appl. Catal., B*, 1995, **5**, 377-387.
122 B. H. J. Bielski, D. E. Cabelli, R. L. Arudi and A. B. Ross, *J. Phys. Chem. B*, 1985, **14**, 1041-1100.
123 A. J. Cowan, J. W. Tang, W. H. Leng, J. R. Durrant and D. R. Klug, *J. Phys. Chem. C*, 2010, **114**, 4208-4214.
124 H. Gerischer and A. Heller, *J. Phys. Chem.*, 1991, **95**, 5261-5267.
125 W. Choi, J. Yeo, J. Ryu, T. Tachikawa and T. Majima, *Environ. Sci. Technol.*, 2010, **44**, 9099-9104.
126 J. Ryu and W. Choi, *Environ. Sci. Technol.*, 2004, **38**, 2928-2933.
127 J. Ryu and W. Choi, *Environ. Sci. Technol.*, 2007, **41**, 6313-6314.
128 D. Monllor-Satoca, T. Tachikawa, T. Majima and W. Choi, *Environ. Sci. Technol.*, 2011, **45**, 2030-2031.
129 D. Monllor-Satoca, R. Gomez and W. Choi, *Environ. Sci. Technol.*, 2012, **46**, 5519-5527.
130 H. Lee and W. Choi, *Environ. Sci. Technol.*, 2002, **36**, 3872-3878.
131 C. Kormann, D. W. Bahnemann and M. R. Hoffmann, *Environ. Sci. Technol.*, 1988, **22**, 798-806.
132 X. Z. Li, C. C. Chen and J. C. Zhao, *Langmuir*, 2001, **17**, 4118-4122.
133 M. Teranishi, S. Naya and H. Tada, *J. Am. Chem. Soc.*, 2010, **132**, 7850-7851.

134 J. Yi, C. Bahrini, C. Schoemaecker, C. Fittschen and W. Choi, *J. Phys. Chem. C*, 2012, **116**, 10090–10097.
135 N. M. Dimitrijevic, B. K. Vijayan, O. G. Poluektov, T. Rajh, K. A. Gray, H. Y. He and P. Zapol, *J. Am. Chem. Soc.*, 2011, **133**, 3964-3971.
136 E. Fujita, *Coord. Chem. Rev.*, 1999, **185-186**, 373-384.
137 T. Yui, A. Kan, C. Saitoh, K. Koike, T. Ibusuki and O. Ishitani, *ACS Appl. Mater. Interfaces*, 2011, **3**, 2594-2600.
138 S. K. Choi, U. Kang, S. Lee, D. J. Ham, S. M. Ji and H. Park, *Adv. Energy Mater.*, 2014, **4**, 1301614.
139 H. Park, H.-H. Qu, A. J. Colussi and M. R. Hoffmann, *J. Phys. Chem. A*, 2015, **119**, 4658-4666.
140 J. R. Bolton, S. J. Strickler and J. S. Connolly, *Nature*, 1985, **316**, 495-500.
141 J. Greeley, T. F. Jaramillo, J. Bonde, I. B. Chorkendorff and J. K. Norskov, *Nat. Mater.*, 2006, **5**, 909-913.
142 S. Trasatti, *J. Electroanal. Chem.*, 1972, **39**, 163-184.
143 T. Hisatomi, K. Miyazaki, K. Takanabe, K. Maeda, J. Kubota, Y. Sakata and K. Domen, *Chem. Phys. Lett.*, 2010, **486**, 144-146.
144 K. Maeda and K. Domen, *Chem. Mater.*, 2010, **22**, 612-623.
145 Y. Park, S. H. Kang and W. Choi, *Phys. Chem. Chem. Phys.*, 2011, **13**, 9425-9431.
146 R. Leary and A. Westwood, *Carbon*, 2011, **49**, 741-772.
147 G. H. Moon, Y. Park, W. Kim and W. Choi, *Carbon*, 2011, **49**, 3454-3462.
148 L.-L. Tan, S.-P. Chai and A. R. Mohamed, *ChemSusChem*, 2012, **5**, 1868-1882.
149 H.-i. Kim, G. H. Moon, D. Monllor-Satoca, Y. Park and W. Choi, *J. Phys. Chem. C*, 2012, **116**, 1535-1543.
150 G. Moon, D. Kim, H. Kim, A. D. Bokare and W. Choi, *Environ. Sci. Technol. Lett.*, 2014, **1**, 185-190.
151 G. Moon, W. Kim, A. D. Bokare, N. Sung and W. Choi, *Energy Environ. Sci.*, 2014, **7**, 4023-4028.
152 H.-i. Kim, S. Kim, J. Kang and W. Choi, *J. Catal.*, 2014, **309**, 49-57.
153 A. J. Hoffman, E. R. Carraway and M. R. Hoffmann, *Environ. Sci. Technol.*, 1994, **28**, 776-785.
154 W. Kim, T. Seok and W. Choi, *Energy Environ. Sci.*, 2012, **5**, 6066-6070.
155 A. J. Bard and M. A. Fox, *Acc. Chem. Res.*, 1995, **28**, 141-145.
156 Y. Park, K. J. McDonald and K.-S. Choi, *Chem. Soc. Rev.*, 2013, **42**, 2321-2337.
157 K. Sivula, F. Le Formal and M. Gratzel, *ChemSusChem*, 2011, **4**, 432-449.
158 F. X. Yin, K. Takanabe, M. Katayama, J. Kubota and K. Domen, *Electrochem. Commun.*, 2010, **12**, 1177-1179.
159 W. Kim, T. Tachikawa, D. Monllor-Satoca, H.-i. Kim, T. Majima and W. Choi, *Energy Environ. Sci.*, 2013, **6**, 3732-3739.
160 N. Lakshminarasimhan, W. Kim and W. Choi, *J. Phys. Chem. C*, 2008, **112**, 20451-20457.
161 Y. Park, W. Kim, D. Monllor-Satoca, T. Tachikawa, T. Majima and W. Choi, *J. Phys. Chem. Lett.*, 2013, **4**, 189-194.
162 N. Lakshminarasimhan, E. Bae and W. Choi, *J. Phys. Chem. C*, 2007, **111**, 15244-15250.
163 S. K. Choi, S. Kim, S. K. Lim and H. Park, *J. Phys. Chem. C*, 2010, **114**, 16475-16480.
164 T. H. Jeon, W. Choi and H. Park, *J. Phys. Chem. C*, 2011, **115**, 7134-7142.
165 J. S. Jang, S. H. Choi, H. Park, W. Choi and J. S. Lee, *J. Nanosci. Nanotechnol.*, 2006, **6**, 3642-3646.
166 S. K. Choi, S. Kim, J. Ryu, S. K. Lim and H. Park, *Photochem. Photobiol. Sci.*, 2012, **11**, 1437-1444.
167 H. W. Jeong, T. H. Jeon, J. S. Jang, W. Choi and H. Park, *J. Phys. Chem. C*, 2013, **117**, 9104-9112.
168 D. Zhao, C. C. Chen, C. L. Yu, W. H. Ma and J. C. Zhao, *J. Phys. Chem. C*, 2009, **113**, 13160-13165.
169 S. Biswas, M. F. Hossain, M. Shahjahan, K. Takahashi, T. Takahashi and A. Fujishima, *J. Vac. Sci. Technol. A*, 2009, **27**, 880-884.
170 W. Smith and Y. P. Zhao, *J. Phys. Chem. C*, 2008, **112**, 19635-19641.
171 L. X. Cao, F. J. Spiess, A. M. Huang, S. L. Suib, T. N. Obee, S. O. Hay and J. D. Freihaut, *J. Phys. Chem. B*, 1999, **103**, 2912-2917.

172 Y. Cao, X. T. Zhang, W. S. Yang, H. Du, Y. B. Bai, T. J. Li and J. N. Yao, *Chem. Mater.*, 2000, **12**, 3445-3448.

173 U. Scharf, M. Schramlmarth, A. Wokaun and A. Baiker, *J. Chem. Soc., Faraday Trans.*, 1991, **87**, 3299-3307.

174 J. H. Fang, J. W. Wu, X. M. Lu, Y. C. Shen and Z. H. Lu, *Chem. Phys. Lett.*, 1997, **270**, 145-151.

175 X. C. Shen, Z. L. Zhang, B. Zhou, J. Peng, M. Xie, M. Zhang and D. W. Pang, *Environ. Sci. Technol.*, 2008, **42**, 5049-5054.

176 H. Park, Y. K. Kim and W. Choi, *J. Phys. Chem. C*, 2011, **115**, 6141-6148.

177 J. S. Jang and H. Park, in *Materials and Processes for Solar Fuel Production*, eds. R. Subramanian, B. Viswanathan and J. S. Lee, Springer, New York, 2014.

178 H. Tada, A. Kokubu, M. Iwasaki and S. Ito, *Langmuir*, 2004, **20**, 4665-4670.

179 W. Smith and Y. P. Zhao, *Catal. Commun.*, 2009, **10**, 1117-1121.

180 B. Tryba, M. Piszcz and A. W. Morawski, *Int. J. Photoenergy*, 2009, **2009**, 297319.

181 J. Papp, S. Soled, K. Dwight and A. Wold, *Chem. Mater.*, 1994, **6**, 496-500.

182 H. Park, K. Y. Kim and W. Choi, *Chem. Commun.*, 2001, 281-282.

183 H. Park, K. Y. Kim and W. Choi, *J. Phys. Chem. B*, 2002, **106**, 4775-4781.

184 R. Abe, H. Takami, N. Murakami and B. Ohtani, *J. Am. Chem. Soc.*, 2008, **130**, 7780-7781.

185 D. X. Shi, Y. Q. Feng and S. H. Zhong, *Catal. Today*, 2004, **98**, 505-509.

186 C. Y. Wang, H. M. Shang, T. Ying, T. S. Yuan and G. W. Zhang, *Sep. Purif. Technol.*, 2003, **32**, 357-362.

187 A. Kumar and A. K. Jain, *J. Photochem. Photobiol., A*, 2003, **156**, 207-218.

188 Y. Bessekhouad, N. Chaoui, M. Trzpit, N. Ghazzal, D. Robert and J. V. Weber, *J. Photochem. Photobiol., A*, 2006, **183**, 218-224.

189 H. B. Yin, Y. Wada, T. Kitamura, T. Sakata, H. Mori and S. Yanagida, *Chem. Lett.*, 2001, 334-335.

190 T. A. Khalyavka, E. I. Kapinus and T. I. Viktorova, *Pol. J. Chem.*, 2008, **82**, 107-112.

191 A. Kumar and A. K. Jain, *J. Mol. Catal., A*, 2001, **165**, 265-273.

192 P. A. Sant and P. V. Kamat, *Phys. Chem. Chem. Phys.*, 2002, **4**, 198-203.

193 H. Matsumoto, T. Matsunaga, T. Sakata, H. Mori and H. Yoneyama, *Langmuir*, 1995, **11**, 4283-4287.

194 H. Tada, T. Mitsui, T. Kiyonaga, T. Akita and K. Tanaka, *Nat. Mater.*, 2006, **5**, 782-786.

195 N. Nishimura, B. Raphael, K. Maeda, L. Le Gendre, R. Abe, J. Kubota and K. Domen, *Thin Solid Films*, 2010, **518**, 5855-5859.

196 R. Ohnishi, M. Katayama, K. Takanabe, J. Kubota and K. Domen, *Electrochim. Acta*, 2010, **55**, 5393-5400.

197 T. Hisatomi, M. Otani, K. Nakajima, K. Teramura, Y. Kako, D. L. Lu, T. Takata, J. N. Kondo and K. Domen, *Chem. Mater.*, 2010, **22**, 3854-3861.

198 M. Tabata, K. Maeda, T. Ishihara, T. Minegishi, T. Takata and K. Domen, *J. Phys. Chem. C*, 2010, **114**, 11215-11220.

199 H.-i. Kim, D. Monllor-Satoca, W. Kim and W. Choi, *Energy Environ. Sci.*, 2015, **8**, 247-257.

200 Y. Park, S. H. Lee, S. O. Kang and W. Choi, *Chem. Commun.*, 2010, **46**, 2477-2479.

201 S. K. Choi, H. S. Yang, J. H. Kim and H. Park, *Appl. Catal., B*, 2012, **121-122**, 206-213.

202 V. H. Houlding and M. Gratzel, *J. Am. Chem. Soc.*, 1983, **105**, 5695-5696.

203 S. Ikeda, C. Abe, T. Torimoto and B. Ohtani, *J. Photochem. Photobiol., A*, 2003, **160**, 61-67.

204 G. Kim and W. Choi, *Appl. Catal., B*, 2010, **100**, 77-83.

205 S. Kim and W. Choi, *J. Phys. Chem. B*, 2005, **109**, 5143-5149.

206 J. M. Notestein, E. Iglesia and A. Katz, *Chem. Mater.*, 2007, **19**, 4998-5005.

207 Y. Park, N. J. Singh, K. S. Kim, T. Tachikawa, T. Majima and W. Choi, *Chem.-Eur. J.*, 2009, **15**, 10843-10850.

208 P. Persson, R. Bergstrom and S. Lunell, *J. Phys. Chem. B*, 2000, **104**, 10348-10351.

209 Y. S. Seo, C. Lee, K. H. Lee and K. B. Yoon, *Angew. Chem., Int. Ed.*, 2005, **44**, 910-913.

210 M. Yang, D. W. Thompson and G. J. Meyer, *Inorg. Chem.*, 2002, **41**, 1254-1262.

211 G. Zhang and W. Choi, *Chem. Commun.*, 2012, **48**, 10621-10623.

212 W. R. Duncan and O. V. Prezhdo, *Annu. Rev. Phys. Chem.*, 2007, **58**, 143-184.

213 E. Bae and W. Choi, *J. Phys. Chem. B*, 2006, **110**, 14792-14799.

214 E. Bae, W. Choi, J. W. Park, H. S. Shin, S. B. Kim and J. S. Lee, *J. Phys. Chem. B*, 2004, **108**, 14093-14101.

215 H. Park and W. Choi, *Langmuir*, 2006, **22**, 2906-2911.
216 H. Park, E. Bae, J. J. Lee, J. Park and W. Choi, *J. Phys. Chem. B*, 2006, **110**, 8740-8749.
217 W. Kim, T. Tachikawa, T. Majima, C. Li, H.-J. Kim and W. Choi, *Energy Environ. Sci.*, 2010, **3**, 1789-1795.
218 D. P. Arnold and J. Blok, *Coord. Chem. Rev.*, 2004, **248**, 299-319.
219 K. Kalyanasundaram, ed., *Photochemistry of Polypyridine and Porphyrin Complexes*, Academic Press, San Diego, 1992.
220 A. G. Agrios, K. A. Gray and E. Weitz, *Langmuir*, 2004, **20**, 5911-5917.
221 T. Tachikawa, S. Tojo, M. Fujitsuka and T. Majima, *J. Phys. Chem. B*, 2004, **108**, 5859-5866.
222 G. Kim, S.-H. Lee and W. Choi, *Appl. Catal., B*, 2015, **162**, 463-469.
223 Y. Cho, H. Kyung and W. Choi, *Appl. Catal., B*, 2004, **52**, 23-32.
224 Y. K. Kim, S. Lee, J. Ryu and H. Park, *Appl. Catal., B*, 2015, **163**, 584-590.
225 H. Wender, A. F. Feil, L. B. Diaz, C. S. Ribeiro, G. J. Machado, P. Migowski, D. E. Weibel, J. Dupont and S. R. Teixeira, *ACS Appl. Mater. Interfaces*, 2011, **3**, 1359-1365.
226 M. C. Wu, J. Hiltunen, A. Sapi, A. Avila, W. Larsson, H. C. Liao, M. Huuhtanen, G. Toth, A. Shchukarev, N. Laufer, A. Kukovecz, Z. Konya, J. P. Mikkola, R. Keiski, W. F. Su, Y. F. Chen, H. Jantunen, P. M. Ajayan, R. Vajtai and K. Kordas, *ACS Nano*, 2011, **5**, 5025-5030.
227 X. Y. Zhang, H. P. Li, X. L. Cui and Y. H. Lin, *J. Mater. Chem.*, 2010, **20**, 2801-2806.
228 B. Zielinska, E. Borowiak-Palen and R. J. Kalenczuk, *Int. J. Hydrogen Energy*, 2008, **33**, 1797-1802.
229 H. Park, A. Bak, A. Y. Ahn, J. Choi and M. R. Hoffmann, *J. Hazard. Mater.*, 2012, **211-212**, 47-54.
230 H. Park, C. D. Vecitis, W. Choi, O. Weres and M. R. Hoffmann, *J. Phys. Chem. C*, 2008, **112**, 885-889.
231 H. Park, C. D. Vecitis and M. R. Hoffmann, *J. Phys. Chem. A*, 2008, **112**, 7616-7626.
232 H. Park, C. D. Vecitis and M. R. Hoffmann, *J. Phys. Chem. C*, 2009, **113**, 7935-7945.
233 J. Kim, W. J. K. Choi, J. Choi, M. R. Hoffmann and H. Park, *Catal. Today*, 2013, **199**, 2-7.
234 S. Y. Yang, W. Choi and H. Park, *ACS Appl. Mater. Interfaces*, 2015, **7**, 1907-1914.
235 T. Sakata, in *Photocatalysis: Fundamentals and Applications*, eds. N. Serpone and E. Pelizzetti, John Wiley & Sons, New York, 1989.
236 E. Borgarello, J. Kiwi, E. Pelizzetti, M. Visca and M. Gratzel, *Nature*, 1981, **289**, 158-160.
237 H. Park and W. Choi, *Catal. Today*, 2005, **101**, 291-297.
238 J. Kim, Y. Park and H. Park, *Int. J. Photoenergy*, 2014, **2014**, 324859.
239 Y.-J. Cho, H.-i. Kim, S. Lee and W. Choi, *J. Catal.*, 2015, **330**, 387-395.
240 S. Bae, S. Kim, S. Lee and W. Choi, *Catal. Today*, 2014, **224**, 21-28.
241 M. Sadeghi, W. Liu, T. G. Zhang, P. Stavropoulos and B. Levy, *J. Phys. Chem.*, 1996, **100**, 19466-19474.
242 G. Khan, Y. K. Kim, S. K. Choi, D. S. Han, A. Abdel-Wahab and H. Park, *Bull. Korean Chem. Soc.*, 2013, **34**, 1137-1144.
243 J. Choi, H. Park and M. R. Hoffmann, *J. Phys. Chem. C*, 2010, **114**, 783-792.
244 J. N. Kondo, D. Nishioka, H. Yamazaki, J. Kubota, K. Domen and T. Tatsumi, *J. Phys. Chem. C*, 2010, **114**, 20107-20113.
245 M. Katayama, D. Yokoyama, Y. Maeda, Y. Ozaki, M. Tabata, Y. Matsumoto, A. Ishikawa, J. Kubota and K. Domen, *Mater. Sci. Eng., B*, 2010, **173**, 275-278.
246 G. L. Chiarello, E. Selli and L. Forni, *Appl. Catal., B*, 2008, **84**, 332-339.
247 J. S. Jang, S. H. Choi, H. G. Kim and J. S. Lee, *J. Phys. Chem. C*, 2008, **112**, 17200-17205.
248 C.-W. Tsai, H. M. Chen, R.-S. Liu, K. Asakura and T.-S. Chan, *J. Phys. Chem. C*, 2011, **115**, 10180-10186.
249 M. Mrowetz and E. Selli, *New J. Chem.*, 2006, **30**, 108-114.
250 J. Kim and W. Choi, *Energy Environ. Sci.*, 2010, **3**, 1042-1045.
251 Y. Cho, H. Park and W. Choi, *J. Photochem. Photobiol., A*, 2004, **165**, 43-50.
252 J. Ryu and W. Choi, *Environ. Sci. Technol.*, 2008, **42**, 294-300.

Table 1. Some outstanding questions and the related topics in charge carrier behaviors in photocatalysis

Questions	Related topics	Research examples
How can the recombination of charge pairs be minimized?	*Metal deposition*	23,37,98,114,241
	Composites with carbon nanomaterials	33,35,145,149,242
	Doping (metals & non-metals)	28,53,54,56,57,243-245
	Electron shuttle	37,85,95
	Interparticle CT systems	160-163,166
	Heterojunctions (binary, tertiary, etc.)	25,26,32
How can multi-electron transfer processes be facilitated?	*Catalysts for hydrogen evolution*	33,35,80,98,145,149,246,247
	Catalysts for oxygen evolution	20,28,29,45
	Catalysts for CO_2 conversion	139,154,248
	Catalysts for H_2O_2 production	82,249
What influences the charge transfer reactions that lead to the generation of reactive oxygen species? Is it possible to control this selectively?	*Fluorination*	75,77,79,80,250
	Phosphonation	76,80
	Ion exchange resin	61,154,215
	Surfactants	223,251
	Polymers	72,211
	Structural engineering (porosity, surface area, nanostructure, etc.)	163,164,166,252
How can visible light photons be utilized to induce CT in photocatalytic systems?	*Doping*	53,54,56,57,243-245
	Dye sensitization	97,98,104,166,201,207,213-217
	Ligand-to-metal charge transfer (LMCT)	204,205,211

Scheme Caption

Scheme 1. Comparison of photocatalytic reaction features for environmental purification versus solar fuel synthesis.

Figure Captions

Fig. 1. Primary reactive oxygen species (ROS) generated in TiO_2 photocatalysis.

Fig. 2. (a, b) Fluorescence images of free hydroxyl radicals ($^{\bullet}OH_f$) that migrated through a gap from the UV-illuminated TiO_2 (a: anatase, b: rutile) to HPF-coated cover glass. The TiO_2/water system with silanol-modified HPF (3'-(*p*-hydroxyphenyl)fluorescein) was compared before (left) and after (right) UV irradiation for 5 sec. The diffusion gap is 7.5 μm. The UV irradiation region is inside the yellow circle in the images. NFI indicates the number of fluorescence signals. The size of the image is 50 × 50 μm. (c) Illustration of OH-radical-mediated photocatalysis on anatase and rutile. Reprinted with permission from Ref. 74 (Copyright 2014 Wiley-VCH Verlag GmbH & Co. KGaA, Weinheim).

Fig. 3. Comparison of Fe^{3+}-mediated photocurrents collected on a Pt electrode for TiO_2 and Pt/TiO_2. The inset shows the current collection on an inert Pt electrode immersed in UV-illuminated Pt/TiO_2 suspension. Adapted with permission from Ref. 150 (Copyright 2014 American Chemical Society).

Fig. 4. (a) Schematic illustration of As(III) as an external charge recombination center on UV-excited TiO_2. (b) Transient absorption time traces (at 700 nm) of TiO_2 slurry in the presence of As(III) or As(V). Reprinted with permission from Ref. 125 (Copyright 2010 American Chemical Society).

Fig. 5. Schematic illustration of the multiple charge transfers occurring in (a) photosynthesis and (b) artificial photosynthesis (Z-scheme).

Fig. 6. (a) Illustration of the various composite structures of TiO_2 and (r)GO sheets and the associated charge transfers for hydrogen production. (b) Photocatalytic H_2 production rates in the aqueous suspensions of TiO_2, TiO_2 dispersed on 2D rGO sheet, and TiO_2/rGO core/shell structure before (left panel) and after Pt loading (right panel). (c) Time profiles of H_2 production in the aqueous suspensions of TiO_2 nanoparticles (NPs), TiO_2 nanofibers (NFs), and GO embedded in TiO_2 NFs (GO-TiO_2 NF). Fig. 6a and 6b adapted with permission from Ref. 149 (Copyright 2012 American Chemical Society). Fig. 6a and 6c reprinted from Ref. 152 with permission by Elsevier.

Fig. 7. Photocatalytic production of H_2O_2 (a) in the presence of 2-propanol and (b) in the absence of 2-propanol as a result of water oxidation. (c) TEM image and EELS mapping of rGO/TiO_2/CoPi. Reproduced from Ref. 151 with permission from The Royal Society of Chemistry.

Fig. 8. (a) Time trend of H_2 evolution in colloidal TiO_2 synthesized using HNO_3 and schematic illustration showing well-dispersed colloidal TiO_2 nanoparticles at pH 2.9 and agglomerated TiO_2 nanoparticles (pH 5.9). Adapted with permission from Ref. 160 (Copyright 2008 American Chemical Society). (b) Schematic illustration and visible light induced production of H_2 in the aqueous suspension of dye/TiO_2/Pt and [dye/TiO_2 + TiO_2 + TiO_2/Pt]. Inset shows the normalized time traces of absorption at 650 nm (Dye•+) during the 532 nm laser photolysis of Dye/TiO_2 without bare TiO_2 and [Dye/TiO_2 + bare TiO_2]. Adapted with permission from Ref. 161 (Copyright 2013 American Chemical Society).

Fig. 9. (a) Time courses of H_2 evolution and photocurrent generations by different TiO_2 photocatalysts and schematic illustration of mesoporous TiO_2 microspheres. Adapted with permission from Ref. 162 (Copyright 2007 American Chemical Society). (b) Time courses of H_2 evolution in aqueous suspensions of TiO_2 nanofibers ($\lambda > 320$ nm) and dye-sensitized TiO_2 nanofibers ($\lambda > 420$ nm) with schematic illustration of mesoporous TiO_2 nanofibers. Reproduced from Ref. 166 with permission from The Royal Society of Chemistry.

Fig. 10. Schematic illustration of the electron-transfer processes in multi-junction systems under UV and visible light. (a) TiO_2/WO_3, (b, c) CdS/TiO_2/Pt, and (d) CdS/TiO_2/WO_3.

Fig. 11. (a) Schematic illustration of charge transfers in *N*-TNT-Ta hybrid. (b) Energy-Filtered TEM (EF-TEM) image of *N*-TNT-Ta hybrid. (c) IPCE spectra of *N*-TNT (triangle) and *N*-TNT-Ta (square) as a function of the incident light wavelength. Dotted lines represent the absorption spectra. (d) Photocurrent transients and the concurrent generation of H_2 and O_2 with *N*-TNT (left panel) and *N*-TNT-Ta (right panel) electrodes polarized at +0.9 V vs. Ag/AgCl under UV illumination ($\lambda > 320$ nm). Reproduced from Ref. 199 with permission from The Royal Society of Chemistry.

Fig. 12. Schematic illustration of (a) dye-sensitization mechanism, (b) sensitization by pre-bound dyes, and (c) sensitization by unbound dyes. Reproduced from Ref. 217 with permission from The Royal Society of Chemistry.

Fig. 13. Schematic illustration of (a) ligand-to-metal charge transfer (LMCT) mechanism, (b) LMCT by phenolic resins, and (c) LMCT with the adsorbates of $C_{60}(OH)_x$. Fig. 13b reproduced from Ref. 211 with permission from The Royal Society of Chemistry. Fig. 13c reprinted with permission from Ref. 207 (Copyright 2009 Wiley-VCH Verlag GmbH & Co. KGaA, Weinheim).

Fig. 14. (a) Applications of charge transfer to the energy-water nexus. Photovoltaic-assisted electrochemical system can effectively remediate water pollutants and deactivate bacteria/virus in the presence of chloride at the anode, while chemical fuels (e.g., H_2) can be produced at the cathode. (b, c) This dual function of the semiconductor can be achieved in particulate (suspension) systems (e.g., F-TiO_2/Pt) without power assistance. Reproduced from Ref. 250 with permission from The Royal Society of Chemistry.

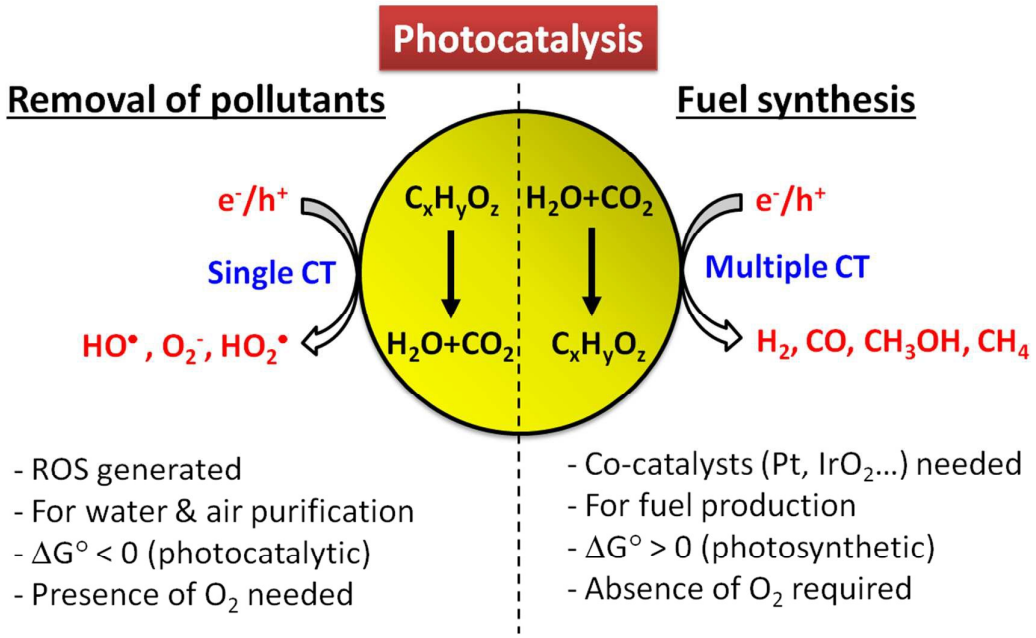

159

160

161 **Scheme 1**. Comparison of photocatalytic reaction features for environmental
162 purification versus solar fuel synthesis.

163

164

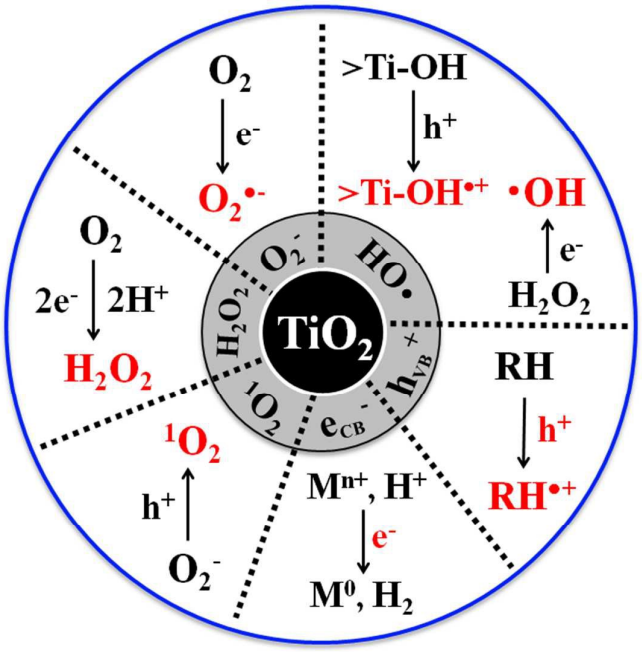

Fig. 1. Primary reactive oxygen species (ROS) generated in TiO_2 photocatalysis.

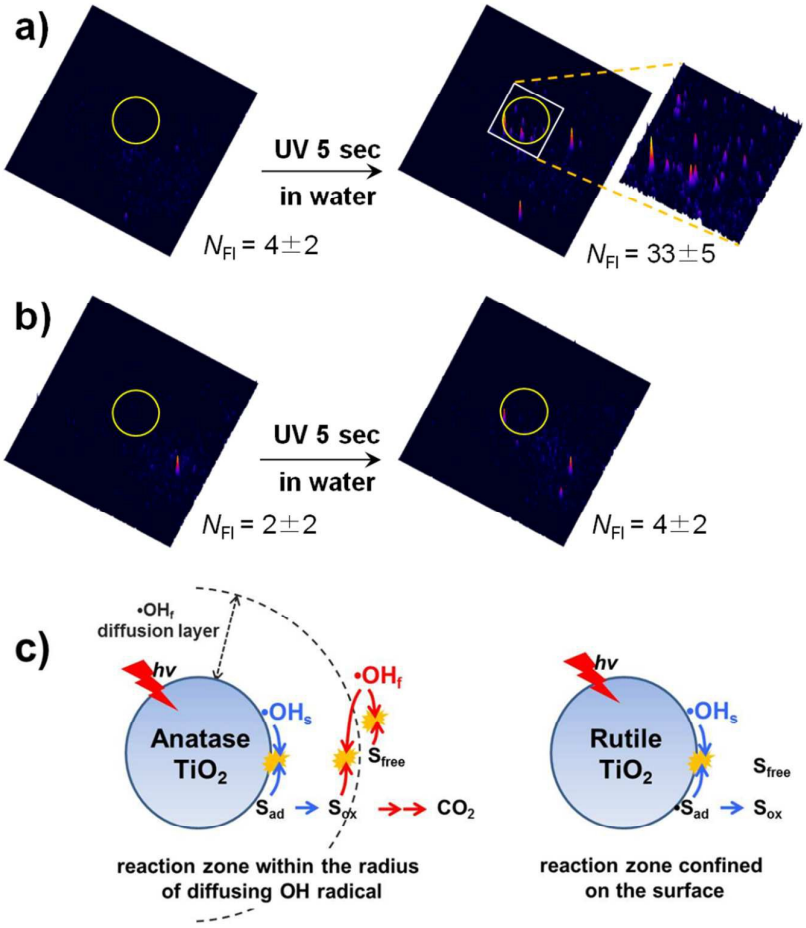

Fig. 2. (a, b) Fluorescence images of free hydroxyl radicals ($^{\bullet}OH_f$) that migrated through a gap from the UV-illuminated TiO_2 (a: anatase, b: rutile) to HPF-coated cover glass. The TiO_2/water system with silanol-modified HPF (3'-(*p*-hydroxyphenyl)fluorescein) was compared before (left) and after (right) UV irradiation for 5 sec. The diffusion gap is 7.5 μm. The UV irradiation region is inside the yellow circle in the images. NFI indicates the number of fluorescence signals. The size of the image is 50 × 50 μm. (c) Illustration of OH-radical-mediated photocatalysis on anatase and rutile. Reprinted with permission from Ref. 74 (Copyright 2014 Wiley-VCH Verlag GmbH & Co. KGaA, Weinheim).

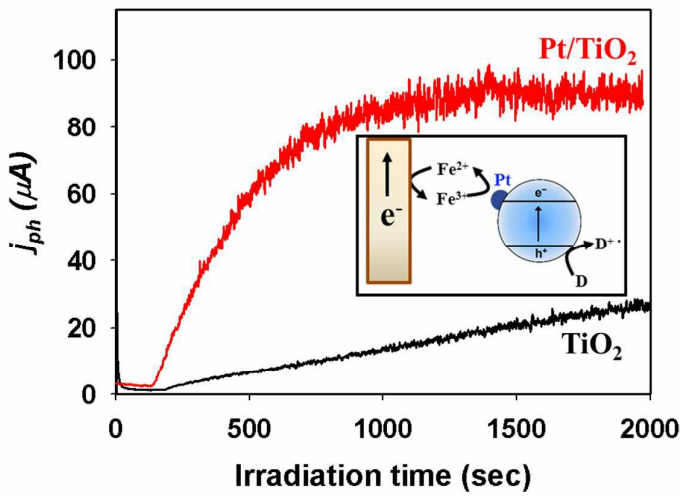

Fig. 3. Comparison of Fe^{3+}-mediated photocurrents collected on a Pt electrode for TiO_2 and Pt/TiO_2. The inset shows the current collection on an inert Pt electrode immersed in UV-illuminated Pt/TiO_2 suspension. Adapted with permission from Ref. 150 (Copyright 2014 American Chemical Society).

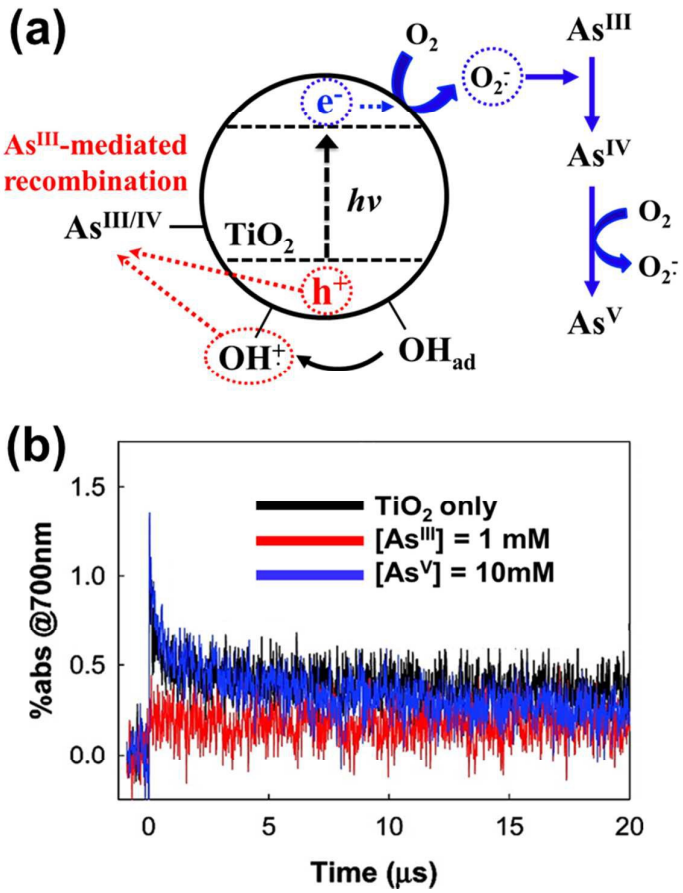

Fig. 4. (a) Schematic illustration of As(III) as an external charge recombination center on UV-excited TiO_2. (b) Transient absorption time traces (at 700 nm) of TiO_2 slurry in the presence of As(III) or As(V). Reprinted with permission from Ref. 125 (Copyright 2010 American Chemical Society).

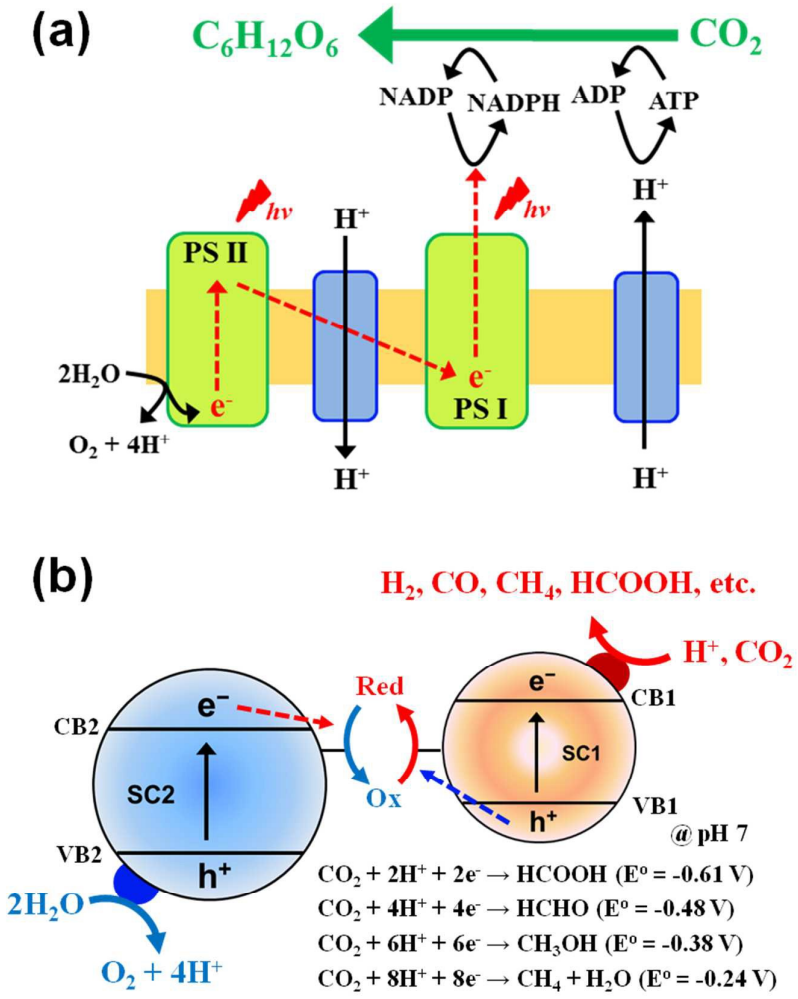

Fig. 5. Schematic illustration of the multiple charge transfers occurring in (a) photosynthesis and (b) artificial photosynthesis (Z-scheme).

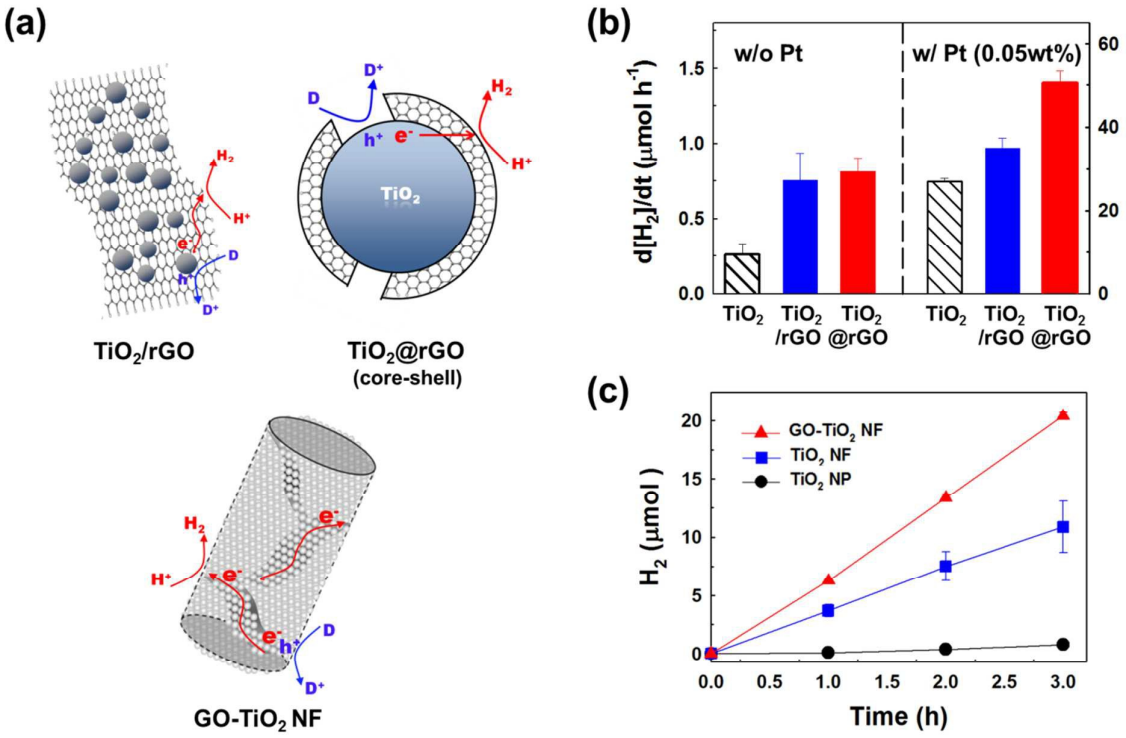

Fig. 6. (a) Illustration of the various composite structures of TiO_2 and (r)GO sheets and the associated charge transfers for hydrogen production. (b) Photocatalytic H_2 production rates in the aqueous suspensions of TiO_2, TiO_2 dispersed on 2D rGO sheet, and TiO_2/rGO core/shell structure before (left panel) and after Pt loading (right panel). (c) Time profiles of H_2 production in the aqueous suspensions of TiO_2 nanoparticles (NPs), TiO_2 nanofibers (NFs), and GO embedded in TiO_2 NFs (GO-TiO_2 NF). Fig. 6a and 6b adapted with permission from Ref. 149 (Copyright 2012 American Chemical Society). Fig. 6a and 6c reprinted from Ref. 152 with permission by Elsevier.

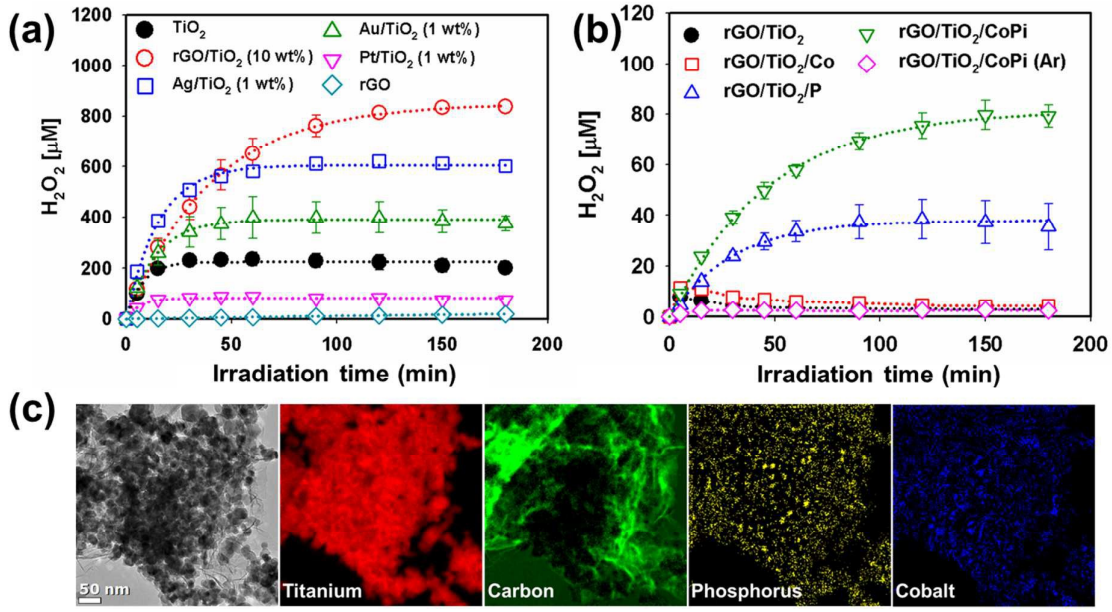

Fig. 7. Photocatalytic production of H_2O_2 (a) in the presence of 2-propanol and (b) in the absence of 2-propanol as a result of water oxidation. (c) TEM image and EELS mapping of rGO/TiO_2/CoPi. Reproduced from Ref. 151 with permission from The Royal Society of Chemistry.

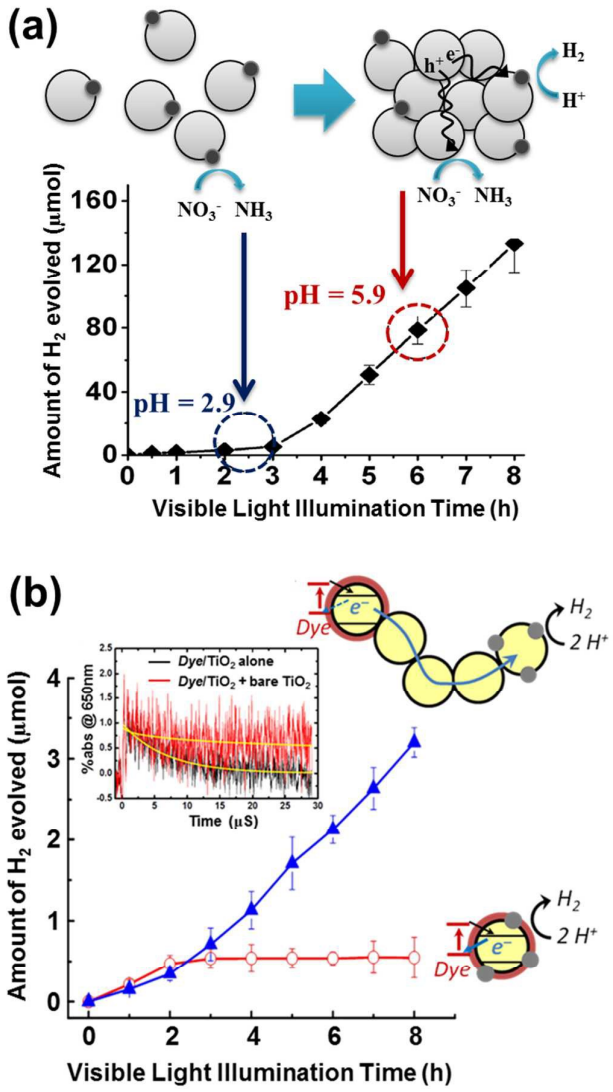

272

273

274 **Fig. 8**. (a) Time trend of H_2 evolution in colloidal TiO_2 synthesized using HNO_3 and
275 schematic illustration showing well-dispersed colloidal TiO_2 nanoparticles at pH 2.9
276 and agglomerated TiO_2 nanoparticles (pH 5.9). Adapted with permission from Ref. 160
277 (Copyright 2008 American Chemical Society). (b) Schematic illustration and visible
278 light induced production of H_2 in the aqueous suspension of dye/TiO_2/Pt and [dye/TiO_2
279 + TiO_2 + TiO_2/Pt]. Inset shows the normalized time traces of absorption at 650 nm
280 (Dye•+) during the 532 nm laser photolysis of Dye/TiO_2 without bare TiO_2 and
281 [Dye/TiO_2 + bare TiO_2]. Adapted with permission from Ref. 161 (Copyright 2013
282 American Chemical Society).

283

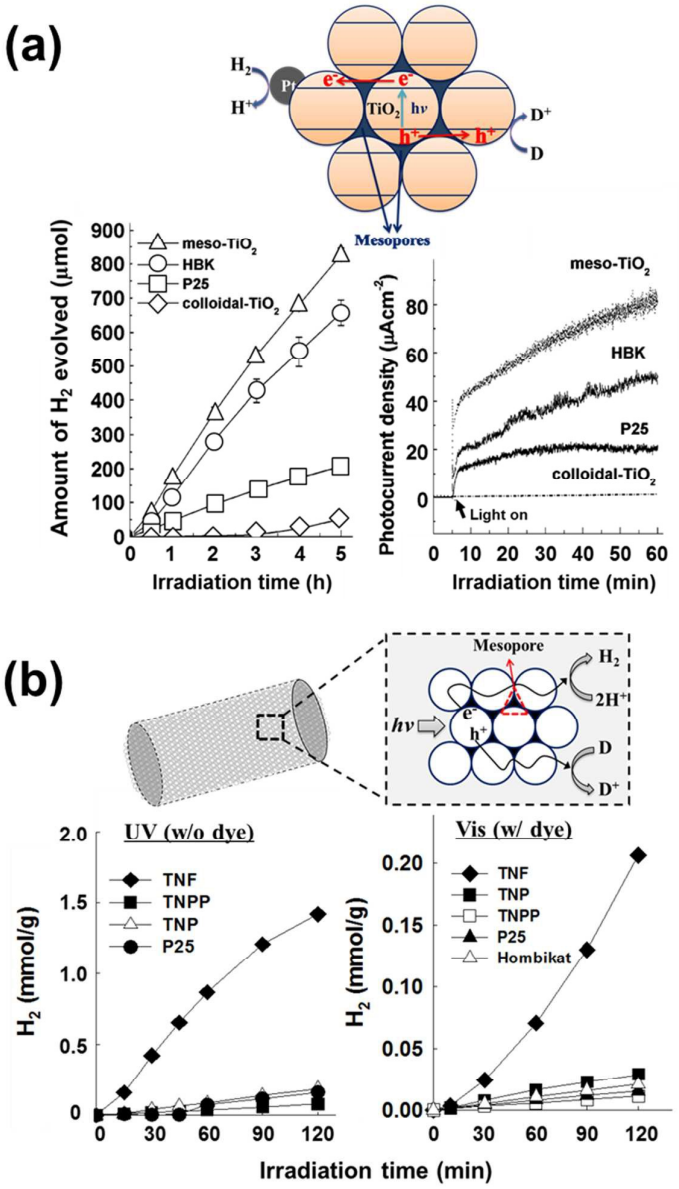

284

285

286 **Fig. 9.** (a) Time courses of H_2 evolution and photocurrent generations by different TiO_2
287 photocatalysts and schematic illustration of mesoporous TiO_2 microspheres. Adapted
288 with permission from Ref. 162 (Copyright 2007 American Chemical Society). (b) Time
289 courses of H_2 evolution in aqueous suspensions of TiO_2 nanofibers ($\lambda > 320$ nm) and
290 dye-sensitized TiO_2 nanofibers ($\lambda > 420$ nm) with schematic illustration of mesoporous
291 TiO_2 nanofibers. Reproduced from Ref. 166 with permission from The Royal Society of
292 Chemistry.

293

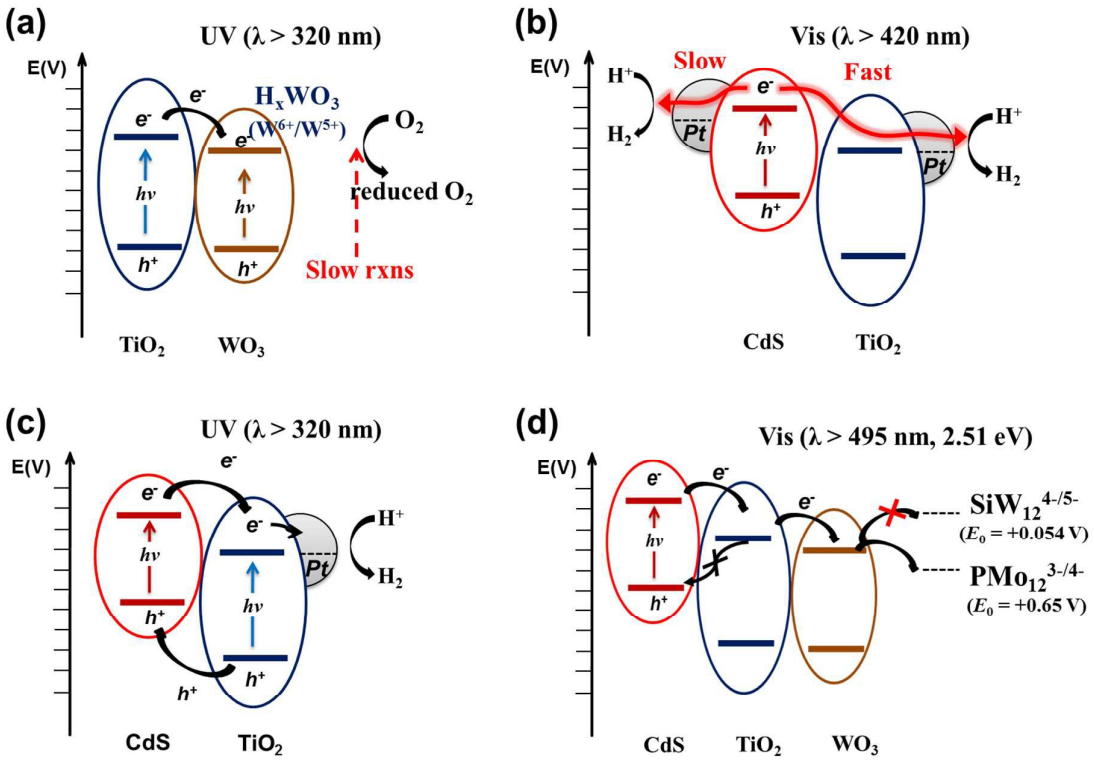

Fig. 10. Schematic illustration of the electron-transfer processes in multi-junction systems under UV and visible light. (a) TiO_2/WO_3, (b, c) $CdS/TiO_2/Pt$, and (d) $CdS/TiO_2/WO_3$.

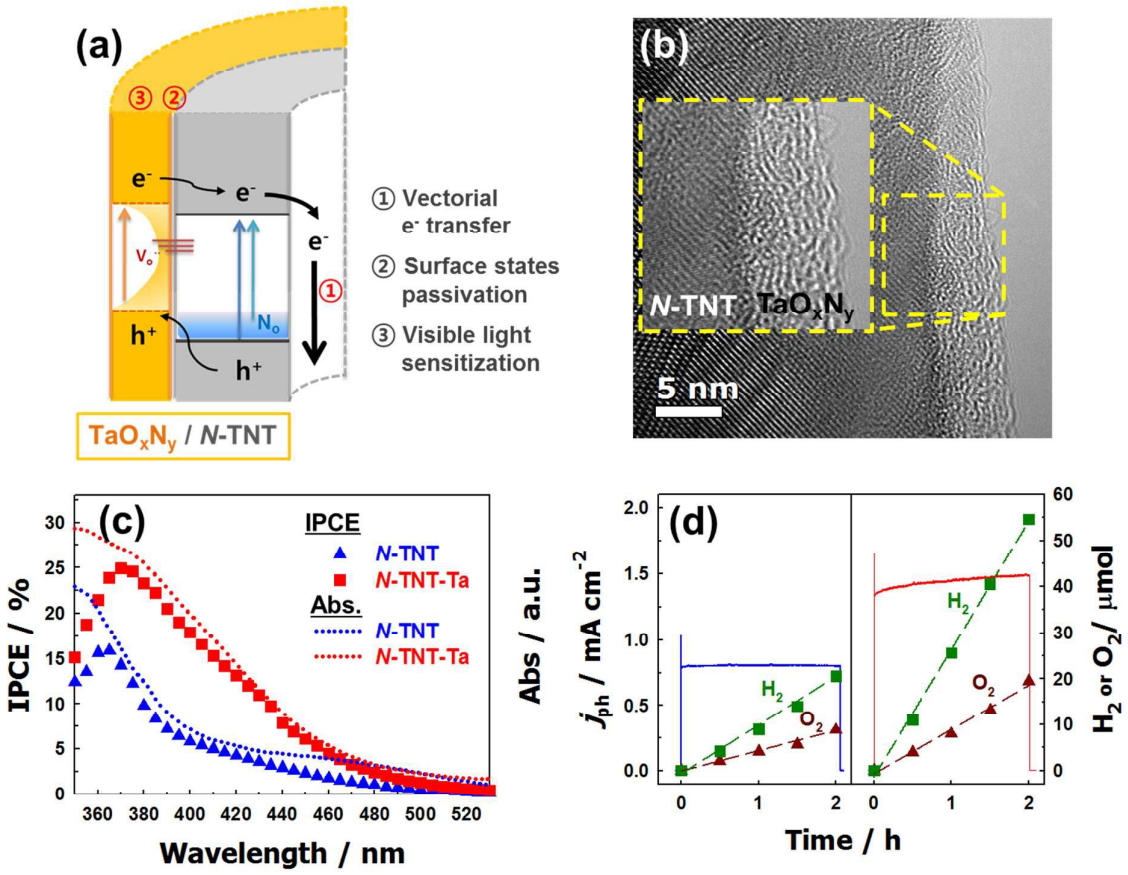

Fig. 11. (a) Schematic illustration of charge transfers in *N*-TNT-Ta hybrid. (b) Energy-Filtered TEM (EF-TEM) image of *N*-TNT-Ta hybrid. (c) IPCE spectra of *N*-TNT (triangle) and *N*-TNT-Ta (square) as a function of the incident light wavelength. Dotted lines represent the absorption spectra. (d) Photocurrent transients and the concurrent generation of H_2 and O_2 with *N*-TNT (left panel) and *N*-TNT-Ta (right panel) electrodes polarized at +0.9 V vs. Ag/AgCl under UV illumination ($\lambda > 320$ nm). Reproduced from Ref. 199 with permission from The Royal Society of Chemistry.

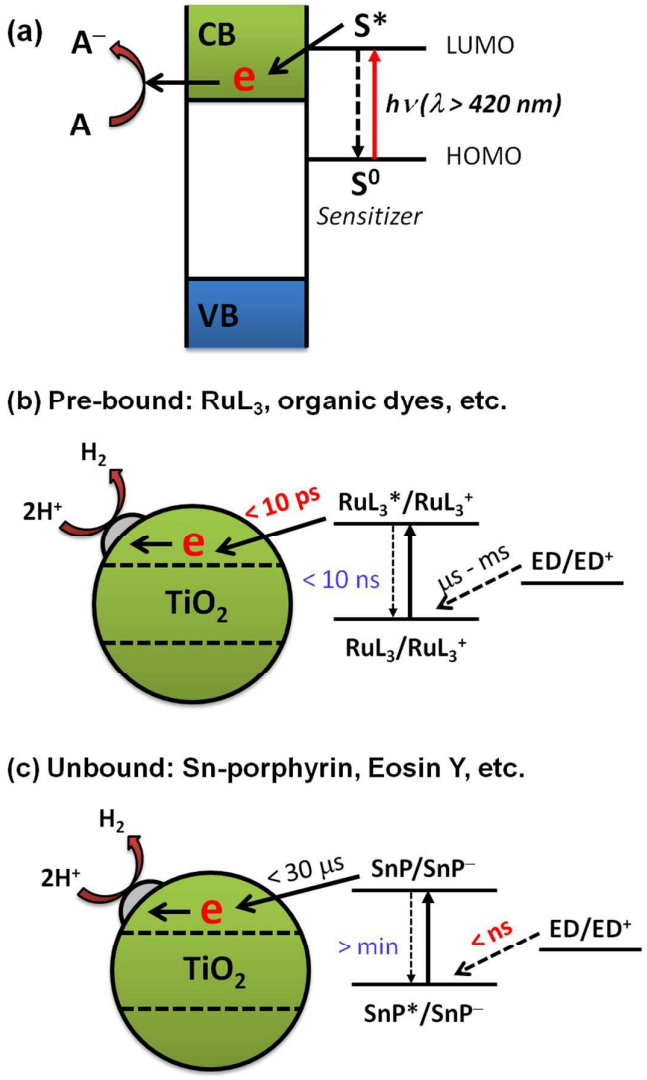

Fig. 12. Schematic illustration of (a) dye-sensitization mechanism, (b) sensitization by pre-bound dyes, and (c) sensitization by unbound dyes. Reproduced from Ref. 217 with permission from The Royal Society of Chemistry.

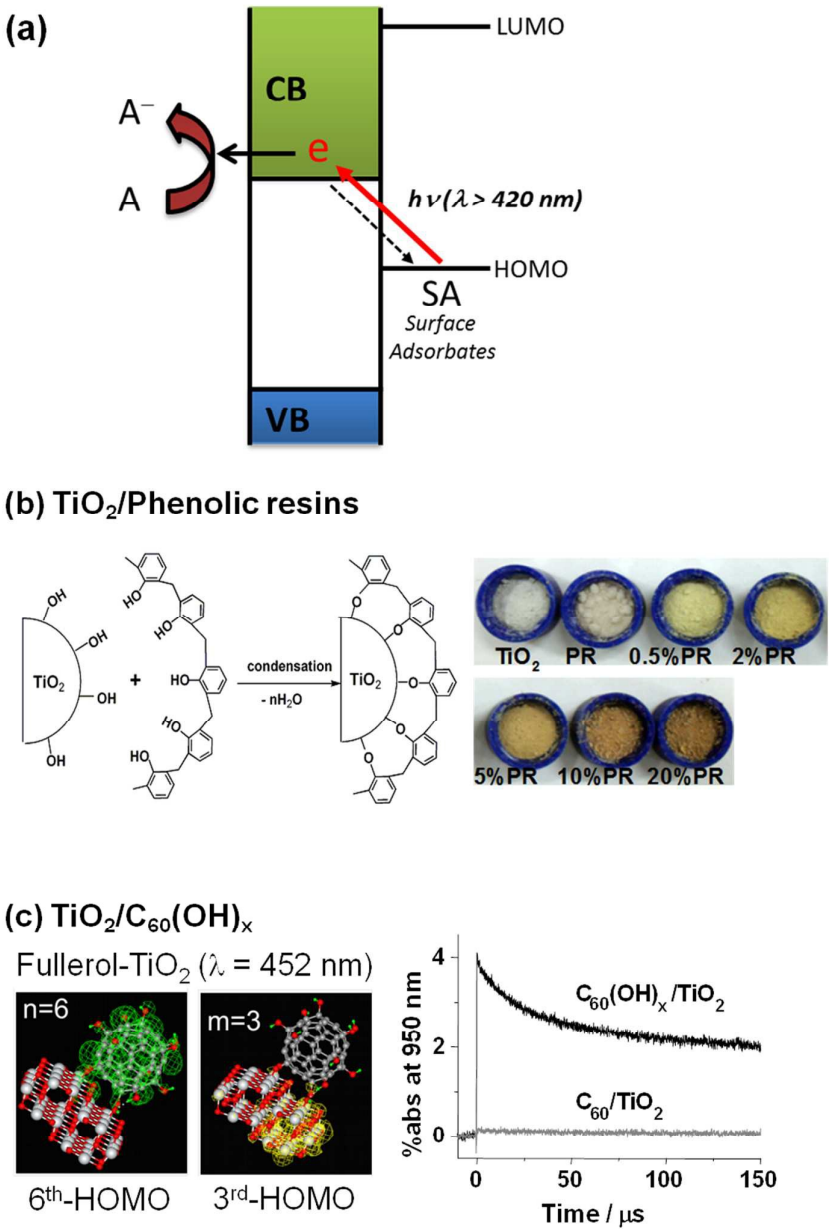

Fig. 13. Schematic illustration of (a) ligand-to-metal charge transfer (LMCT) mechanism, (b) LMCT by phenolic resins, and (c) LMCT with the adsorbates of $C_{60}(OH)_x$. Fig. 13b reproduced from Ref. 211 with permission from The Royal Society of Chemistry. Fig. 13c reprinted with permission from Ref. 207 (Copyright 2009 Wiley-VCH Verlag GmbH & Co. KGaA, Weinheim).

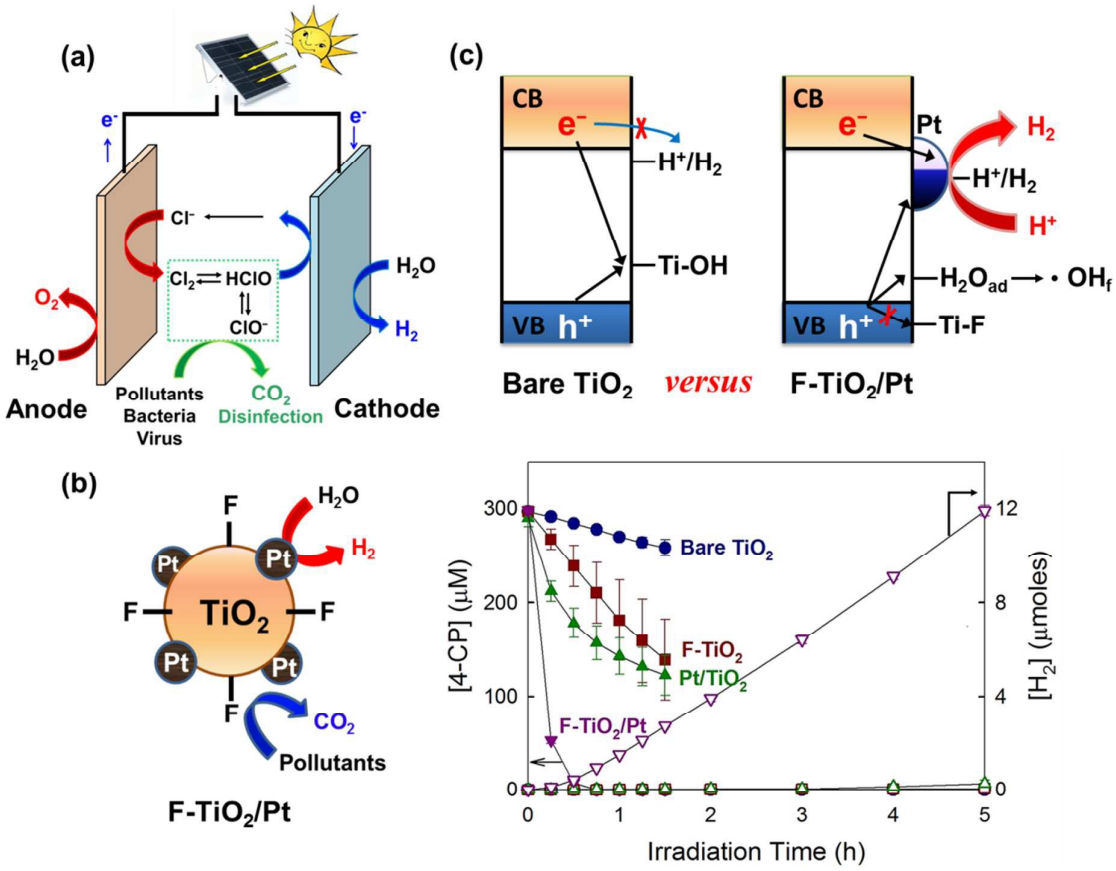

342

343

344 **Fig. 14**. (a) Applications of charge transfer to the energy-water nexus. Photovoltaic-
345 assisted electrochemical system can effectively remediate water pollutants and
346 deactivate bacteria/virus in the presence of chloride at the anode, while chemical fuels
347 (e.g., H_2) can be produced at the cathode. (b, c) This dual function of the semiconductor
348 can be achieved in particulate (suspension) systems (e.g., F-TiO_2/Pt) without power
349 assistance. Reproduced from Ref. 250 with permission from The Royal Society of
350 Chemistry.

351

352

353

354

355

356 **Table of Content**

357

358

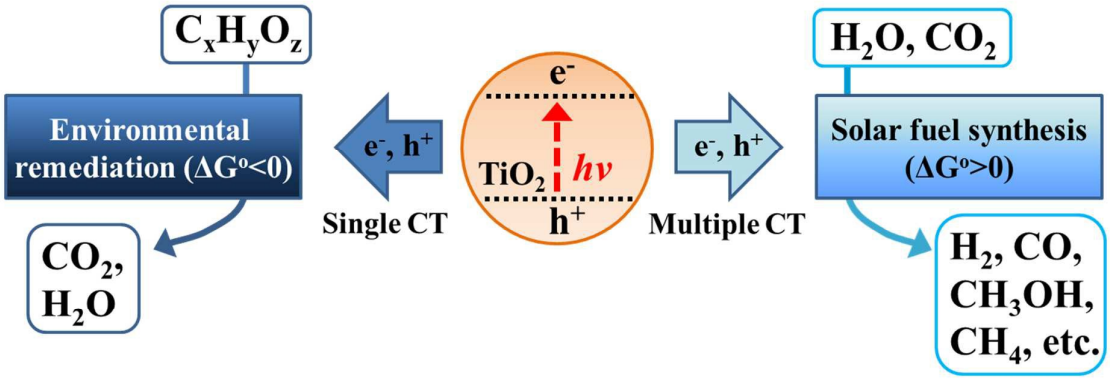

359

Authors' Biographies

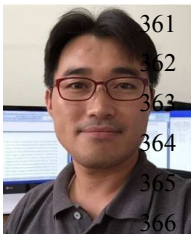

Hyunwoong Park received a B.S. in Environmental Science at Hallym University in 1999 and a Ph.D. degree (advisor: Wonyong Choi) in Environmental Engineering at POSTECH (Pohang, Korea) in 2004. After postdoctoral research at the California Institute of Technology (Pasadena, California: 2006 – 2008), he moved to the School of Energy Engineering at Kyungpook National University (Daegu, Korea) as an assistant professor (2008) and was then promoted to associate professor (2012). He has published over 80 papers in peer-reviewed journals, which have been cited over 4500 times. He was awarded the Knowledge Creativity Award by the Ministry of Education, Science, and Technology, Korea (2012), and the Best Paper Award by the Korean Electrochemical Society (2013). He is serving as the Editor of *Materials Science in Semiconductor Processing* (Elsevier, since 2015) and the Associate Editor of *Environmental Engineering Research* (Korean Society of Environmental Engineers, since 2014). He is also on the editorial advisory boards of *Journal of Environmental Chemical Engineering* (Elsevier, since 2013) and *International Journal of Photoenergy* (Hindawi, since 2014).

Hyoungil Kim received a B.S. in Environmental Engineering at Inha University (Incheon, Korea) in 2008 and a Ph.D. degree (advisor: Wonyong Choi) in Environmental Engineering at POSTECH (Pohang, Korea) in 2014. He spent a half year at POSTECH as a postdoctoral researcher and is currently working in Chemical and Environmental Engineering at Yale University (New Haven, U.S.A) as a postdoctoral researcher.

Gun-hee Moon received a B.S. in Chemical Engineering at Inha University (Incheon, Korea) in 2008, an M.S. degree in Environmental Engineering from POSTECH in 2011, and a Ph.D. degree (advisor: Wonyong Choi) in Chemical Engineering from POSTECH (Pohang, Korea) in 2015. He joined the Materials Science Division of Pacific Northwest National Laboratory (Richland, Washington) as an Alternate Sponsored Fellowship (2011-2012). He is currently working as a postdoctoral researcher in Prof. Choi's laboratory.

Wonyong Choi received a B.S. in engineering from Seoul National University (Seoul, Korea) in 1988, an M.S. in chemistry from POSTECH in 1990, and a Ph.D. in chemistry from California Institute of Technology in 1996. After postdoctoral research in atmospheric chemistry at NASA/Caltech Jet Propulsion Laboratory (1996-98), he joined the faculty of the School of Environmental Science and Engineering, POSTECH as an assistant professor (1998), and was promoted to associate professor (2003), and full professor (2008). His research interests are mainly focused on semiconductor photocatalysis and photochemistry for solar energy conversion and environmental applications, advanced oxidation processes, and environmental chemistry. He has published over 230 papers in peer-reviewed journals, which have been cited over 23,000 times (H-index 59, Web of Science) to date. He received the Young Scientist Award (2006) and the KAST Science and Technology Award (2015) from the Korean Academy of Science and Technology (KAST), Lectureship Award from the Japanese Photochemistry Association (2008), Rising Star faculty fund from POSTECH (2011), Namgo chair professorship from POSTECH (2012) and was elected as Fellow of KAST and Fellow of Royal Society of Chemistry (FRSC) in 2014. Currently, he is serving as the Editor of *Journal of Hazardous Materials* (Elsevier, 2008-). He has been also on the editorial advisory boards of *Energy and Environmental Science* (RSC, 2008-), *Environmental Science and Technology* (ACS: 2015-), and *Journal of Physical Chemistry* (ACS: 2009-2011).